NASA TECHNICAL NOTE

NASA TN D-7704

NASA TN D-7704

INVESTIGATION OF AN ANOMALOUS FLOW CONDITION OF THE LANGLEY PILOT MODEL EXPANSION TUBE

by Wilfred J. Friesen

Langley Research Center

Hampton, Va. 23665

NATIONAL AERONAUTICS AND SPACE ADMINISTRATION • WASHINGTON, D. C. • AUGUST 1974

1. Report No.	2. Government Accession No.	3. Recipient's Catalog No.
NASA TN D-7704		

4. Title and Subtitle	5. Report Date
INVESTIGATION OF AN ANOMALOUS FLOW CONDITION OF THE LANGLEY PILOT MODEL EXPANSION TUBE	August 1974
	6. Performing Organization Code
7. Author(s)	8. Performing Organization Report No.
Wilfred J. Friesen	L-9633
	10. Work Unit No.
9. Performing Organization Name and Address	502-27-01-03
NASA Langley Research Center Hampton, Va. 23665	11. Contract or Grant No.
	13. Type of Report and Period Covered
12. Sponsoring Agency Name and Address	Technical Note
National Aeronautics and Space Administration Washington, D.C. 20546	14. Sponsoring Agency Code

15. Supplementary Notes

16. Abstract

Free-stream flow velocity measurements were made in the Langley pilot model expansion tube during the test flow interval. During this interval, an anomalous dip in pitot pressure occurs for the expansion tube operating conditions employed. Within the test flow interval, the main conclusions reached from comparison of the measured flow velocity, pitot pressure, and tube wall pressure are: the variations which occur in velocity and wall pressure are small compared with the variations in pitot pressure; a corresponding dip in the derived flow density is associated with the dip in pitot pressure; and the value of the average density over the interval, which results from the expansion from the shocked intermediate chamber condition, is approximately one-half of the value that can result from only an isentropic process.

17. Key Words (Suggested by Author(s))	18. Distribution Statement
Expansion tube Velocity measurement Pitot pressure dip Density	Unclassified – Unlimited STAR Category 12

19. Security Classif. (of this report)	20. Security Classif. (of this page)	21. No. of Pages	22. Price*
Unclassified	Unclassified	44	$3.25

*For sale by the National Technical Information Service, Springfield, Virginia 22151

INVESTIGATION OF AN ANOMALOUS FLOW CONDITION OF THE LANGLEY PILOT MODEL EXPANSION TUBE

By Wilfred J. Friesen
Langley Research Center

SUMMARY

Free-stream flow velocity measurements were made in the Langley pilot model expansion tube during the test flow interval. During this interval, an anomalous dip in pitot pressure occurs for the expansion tube operating conditions employed. Within the test flow interval, the main conclusions reached from comparison of the measured flow velocity, pitot pressure, and tube wall pressure are: the variations which occur in velocity and wall pressure are small compared with the variations in pitot pressure; a corresponding dip in the derived flow density is associated with the dip in pitot pressure; and the value of the average density over the interval, which results from the expansion from the shocked intermediate chamber condition, is approximately one-half of the value that can result from only an isentropic process.

INTRODUCTION

An expansion tube is an impulse device which produces a short-duration, hypersonic test flow with flow properties suitable for the study of problems related to planetary entry. The results of an exploratory study of the performance of the Langley pilot model expansion tube are reported in reference 1.

In reference 1, an unexpected decrease or dip in the pitot pressure was reported. The pitot pressure dip occurs within the test flow time interval for certain operating conditions of the expansion tube and seriously reduces the normally short testing time of the facility. Interpretations of this dip in pitot pressure depended on the assumptions made concerning the test flow velocity and density. The velocity of the interface (which is the first flow boundary of the test flow to arrive at the test location) was measured, but measurements of flow velocity within the subsequent test flow were not available to Jones and Moore. (See ref. 1.)

The purpose of the present investigation was to derive the flow density associated with an anomalous flow condition from measured values of the test flow velocity on the tube center line, pitot pressure, and tube wall pressure. Although specifically directed toward a better understanding of the nature of the anomalous flow, this investigation is

part of an effort directed toward understanding the cause of the anomaly. The scope of the present investigation was limited to one initial operating condition of the expansion tube for which a significant pitot pressure dip occurred within the nominal test flow time interval; and only nitrogen was used as the test medium (similar pitot pressure dips are observed for other test gases as well). Also a necessary part of the present investigation was the development of a method of measuring the flow velocity.

The results of the measurements of flow velocity, pitot pressure, tube wall pressure, interface velocity, and shock velocity that were obtained for a specific anomalous flow condition of the expansion tube are presented. Also presented are results which were derived from the measured values. These results include the density, temperature, integrated flux, and the reproducibility of several of the flow properties of the expansion tube cycle.

The magnitudes of the flow properties of an expansion tube can be varied over large ranges. To aid the reader who may be unfamiliar with the nominal magnitudes and trends encountered in expansion tube flows, the predictions of a simple, highly idealized flow model are presented.

SYMBOLS

a	speed of sound
I	intensity
I_0	initial intensity
M	flow Mach number
n	number of expansion tube runs
p	static pressure
p_t	pitot pressure
p_w	tube wall pressure
T	temperature
t	time

$t_{c,1}, t_{c,2}$ times corresponding to positions 1 and 2

$\Delta t_c = t_{c,2} - t_{c,1}$

t_p time corresponding to peak intensity

$U_{s,1}$ velocity of primary (nitrogen) shock wave

u flow velocity

u_i interface velocity

$\bar{u}_{i,p}$ average interface velocity for pressure runs

u_m measured flow velocity

x_1, x_2 positions 1 and 2 (slit centers)

$\Delta x = x_2 - x_1$

γ specific heat ratio

ρ density

σ standard deviation from the mean

$\bar{\sigma}$ estimated variance of the mean

Subscripts:

1, 2, 5, 10, 20 refer to flow regions indicated in figure 1

IDEALIZED MODEL OF FLOW CYCLE

A definition and description of an expansion tube, its operating flow cycle, theoretical basis and performance capability are discussed in reference 2.

In this section an idealized model of an expansion tube flow cycle is briefly sketched and some of the predicted flow properties are stated. This one-dimensional model assumes perfect gases, nonviscous flow, isentropic expansions, no mixing of gases, and

idealized diaphragms. The predictions of this model are presented primarily as a guide to indicate only the expected magnitudes and trends for an ideally operating expansion tube.

Flow Cycle

A distance-time diagram of an idealized flow model is shown in figure 1. Initially, three gases are at rest in three chambers, which are defined by two diaphragms in a constant area tube. The flow cycle is initiated by the rupture of the first diaphragm.

After the rupture of the first diaphragm, the flow cycle, up to the second diaphragm, is that of an ideal shock tube. The expansion of the hydrogen driver gas results in the compression and acceleration of nitrogen within the intermediate chamber at a constant supersonic rate. The flow velocity and state properties of the nitrogen throughout region (2) are constant. Region (2) is bounded by the nitrogen shock and the nitrogen-hydrogen interface (contact surface). The secondary diaphragm ruptures upon arrival of the shock wave.

After the rupture of the second diaphragm, the velocity of the nitrogen-hydrogen interface remains constant as the moving nitrogen expands into the acceleration chamber. For a brief time the flow cycle in the acceleration chamber can be viewed as a shock tube cycle with the nitrogen "driver" initially in motion. Since the motion of the nitrogen is supersonic, the upstream facing expansion wave which moves into region (2) is washed downstream. The test gas is that portion of the nitrogen which has expanded into region (5). Throughout this region the nitrogen flow velocity and state properties are constant. Region (5) is bounded by the helium-nitrogen interface (contact surface) and the tail of the expansion fan.

The role of the helium acceleration gas is to provide a boundary which moves at constant velocity and limits the expansion of the nitrogen to a finite constant pressure p_5. The conditions of constant velocity and pressure require that the work done on the boundary should proceed at a constant rate. For this idealized model, the necessary boundary work is accomplished by continual compression and acceleration of helium at a supersonic rate using the nitrogen test gas (region (5)) and the compressed helium (region (20)) as the contacting or pressure transmitting media.

Flow Properties

The following sequence of flow properties is predicted for an observer located at the test section. Flow begins with the arrival of the helium shock. A helium flow with constant velocity and constant state properties is observed until all the helium, which was initially located between the second diaphragm and the test section, has passed the test section; the nitrogen test flow with constant velocity and constant state properties is now

observed until the test flow is terminated by the arrival of the tail of the expansion fan. After the arrival of the expansion fan, the flow properties of the nitrogen are no longer constant with the passage of time. During the passage of the expansion fan the flow velocity decreases and the state properties increase monotonically.

In general, the following relations between the helium flow and the nitrogen test flow are observed at the test section:

$$u_{20} = u_i = u_5 = \text{Constant}$$

$$p_{20} = p_5 = \text{Constant}$$

$$\rho_{20} \neq \rho_5$$

$$T_{20} \neq T_5$$

Since the expansion of the nitrogen from region (2) to region (5) is assumed to be an isentropic process,

$$\frac{\rho_5}{\rho_2} = \left(\frac{p_5}{p_2}\right)^{1/\gamma} = \left(\frac{T_5}{T_2}\right)^{\frac{1}{\gamma-1}} = \left(\frac{a_5}{a_2}\right)^{\frac{2}{\gamma-1}} \tag{1}$$

The relation between the flow velocities in region (2) and region (5) for the one upstream facing expansion wave, which is given in reference 2, is

$$\frac{2}{\gamma - 1} a_2 + u_2 = \frac{2}{\gamma - 1} a_5 + u_5 \tag{2}$$

APPARATUS

Expansion Tube

The Langley pilot model expansion tube has been completely described in reference 1. Only one set of chamber lengths and one set of gases and initial pressures were used in this investigation. The gases used in the driver, in the intermediate chamber, and in the acceleration chamber were, respectively, room temperature hydrogen, nitrogen, and helium. The first diaphragm was a scribed, 1.59-mm-thick steel diaphragm and the second, a 0.0064-mm-thick mylar diaphragm. At the test section the flow exited as a free jet and subsequently entered a large dump tank. The dimensions and initial operating conditions for the tube are given in table I.

Measurement Apparatus

Tube instrumentation.- The expansion tube instrumentation that was used to detect wave passage and provide trigger signals has been described in reference 1. Ion gaps and pressure gages were used to detect the nitrogen shock in the intermediate chamber; pressure gages were used to detect the helium shock in the acceleration chamber. A microwave antenna located downstream of the test section was used to track the helium-nitrogen interface in the acceleration chamber. A photodetector was used to detect the arrival of the helium-nitrogen interface at the test section.

Improvements to the facility vacuum system, instrumentation, and operating procedure have occurred since the exploratory work reported in reference 1, and have resulted in improved measurement of the initial helium pressure and a substantial reduction in the contamination level of the helium. With regard to contamination, for example, no light was observed from stagnated regions of the helium flow during any of the tube runs. Use of an improved absolute pressure gage resulted in a reproducible filling of the acceleration chamber with the low pressure helium; the pressure gage was of the capacitance diaphragm type.

Flow pressure.- Piezoelectric pressure transducers were used in the measurements of tube wall pressure and pitot pressure. The wall pressure gage was located approximately 26 cm upstream of the test section and was mounted flush with the tube wall. The unfiltered signal from this transducer was recorded by an oscilloscope. The pitot pressure probe was located at the test section on the tube center line. The probe, which had an external diameter of 0.95 cm, shielded the transducer from particles in the flow. The signal from this transducer was processed through a passive filter to suppress frequencies above 50 kHz and then recorded by an oscilloscope. The locations of the pressure probes relative to the exit of the expansion tube are shown in figure 2.

Flow velocity.- A necessary part of this investigation was the development of a method of measuring the flow velocity suitable for the flow conditions to be encountered. The method used consisted of producing a luminous region within the flowing gas, and then, by means of photodetectors, observing the time of arrival of the region at two fixed downstream positions in the flow field. This method is similar to those reported in references 3 and 4. The specific differences are primarily involved with the techniques for producing the luminous regions. In the present investigation a localized region in the flow was excited to luminescence by passing a short duration (10^{-7} sec) current pulse through a previously ionized column in the gas. The ionized column was formed by photoionization just prior to its excitation. Photoionization was used to identify or define a region within the flowing gas for the velocity measurements reported in reference 5; however, the method employed to detect the subsequent location of the defined region was

not applicable to the larger flow densities encountered in the present investigation. Since, for these larger densities, the ionization produced decreases rapidly with distance from the photon source, it was necessary to employ a spacing of about 2.5 cm between the photon source and the exciting electrode and to design both of these components to operate within the boundary of the flow field.

A schematic drawing of the windowless ultraviolet light source used to photoionize the column is shown in figure 3. Ultraviolet light (UV) was produced by means of a constricted electrical discharge in the nylon capillary which was 0.78 mm in diameter and 1.6 cm long. The light duration was of the order of 10^{-7} second. Light from the capillary was partially collimated by a 0.78-mm-diameter field stop. The collimator assembly also served as the electrostatic shielding and was operated at ground potential. The exciting electrode consisted of a 0.5-mm-diameter tungsten wire. The distance between the exciting electrode and the exit collimator of the light source was 2.2 cm. The light source and electrode were located in a plane through the expansion tube center line, and their locations relative to the exit of the expansion tube are shown in figure 2.

A circuit diagram of the transmission line pulse generator which provided pulses to both the light source and exciting electrode is shown in figure 4. The generator produced a pulse of about 10^{-7} second duration. About 4 joules were stored in the coaxial transmission lines when charged to 40 000 volts. The two pulses were derived from the same pulse generator in order to insure proper synchronization between photoionization and excitation of the gas column. The pulse to the exciting electrode was delayed about 10^{-7} second with respect to the pulse to the light source by means of an additional length of coaxial cable.

The passage of the luminous column at two fixed positions in the flow field was detected by two photodetectors (type 931-A); these photodetectors were located behind rectangular slits. The optical arrangement used is shown in figure 5. This optical arrangement effectively placed two rectangular slits (1.59 mm wide, 3.13 mm long, and 1.905 cm apart) in a plane through the center line of the expansion tube. The upstream slit was located 1.3 cm downstream of the photoionizing source. The lens was used at a magnification of two and had a focal length of 17.8 cm and an aperture stop of f/2.5.

An optical filter was used to block radiation to the photodetectors in the wavelength region below 5000 Å, in order to remove radiation due to the first negative band system of the excited N_2^+ ion. Radiation from this band system normally accounts for a large fraction of the light emitted from an electrical discharge in nitrogen. From the standpoints of photodetector overload requirements and interpretation of the data, the combined high intensity and rapid decay associated with this radiation was undesirable for the present application.

The photodetector outputs were terminated in 50-ohm load resistors, and their signals were recorded on two channels of an oscilloscope. An overall rise time of about 10^{-7} second is estimated for the photodetector system. Within the range of light intensities encountered, the responses of the photodetectors were nonlinear to changes in light intensity.

DATA ANALYSIS

The measured results presented in this paper represent average values obtained from 30 expansion tube runs for a single operating condition. Of these, 4 runs were used to obtain wall pressure and pitot pressure data, and 26 runs were used to obtain flow velocity data. A tube run was required for each determination of flow velocity. The flow velocity measurements were made during the nitrogen flow at seven nominal times following the passage of the helium-nitrogen interface. At least two expansion tube runs were made for each nominal time; the reproducibility of the nominal time locations was about ±5 μsec.

Since small variations occurred in the opening of the primary diaphragm, a means of comparing the flow velocities obtained from different expansion tube runs was required. The variation in the measured helium-nitrogen interface velocity u_i was used to characterize the resultant variation in the measured flow velocity u_m due to variation in the primary diaphragm opening. Each measured velocity determination u_m was normalized by the corresponding measured interface velocity u_i, and then multiplied by the average interface velocity $\bar{u}_{i,p}$ obtained for the four pressure runs. The average velocity u which is presented for each of the time locations was obtained from

$$u = \overline{\frac{u_m}{u_i}\,\bar{u}_{i,p}}$$

The standard deviation from mean interface velocity for the four pressure runs was ±0.8 percent. The standard deviation for the 30 runs was ±2 percent. No normalization correction was applied to the pressure data.

Pressure

Sample data oscillograms of the tube wall pressure and pitot pressure are shown in figure 6. The data were reduced to numerical form for computation at time increments of 5 μsec.

Calibration of gages.- The two pressure gages were calibrated by relating the initial rise of the transducer signals to the corresponding pressure changes associated with the passage of a normal helium shock in the acceleration chamber. The pressure changes

were calculated by use of the adiabatic relations for a normal shock given in reference 6. The required inputs to the calculations were the initial conditions of the helium and the measured helium shock velocity. Helium was assumed to behave as a perfect gas. Because of the finite rise time of the transducer signals, the initial signal values following shock arrival were obtained by linearly extrapolating the trend of the signal data to the time of shock arrival (t = 0). For the extrapolations, data were used in the range of 5 to 55 μsec for the wall pressure gage and 50 to 150 μsec for the pitot pressure gage. The standard deviations from the mean values obtained for the four expansion tube runs were: ±1 percent for the two pressure changes, ±1.5 percent for the wall pressure calibration factor, and ±3 percent for the pitot pressure calibration factor.

Possible systematic errors.- The largest uncertainties in the reported pitot and wall pressure measurements are expected to be of a systematic nature. Uncertainties in the degree of validity of at least two assumptions required in the gage calibration, lead to possible systematic errors of the order of 10 percent. It is possible that the values reported for the tube wall pressure and pitot pressure associated with the nitrogen flow may be as much as 10 percent larger than the true pressures.

It was assumed that the pressure response of the gages was linear over the entire range of pressure levels encountered by the gages. A nonlinear behavior would be expected to introduce the larger error in the pitot pressure measurements, since this probe encounters a much larger change in pressure level because of the change from helium to nitrogen flow. The pressure levels associated with the helium flow were below the pressure range for which the linearity of gages of this type had been tested. A possible systematic error in a range from 0 to 10 percent for pitot pressure measurements during the nitrogen flow was estimated from extrapolation of linearity data for gages of the same type.

It was assumed that the tube wall pressure was equal to the free-stream static pressure on the tube center line. The degree to which this assumption is valid is not known. The degree of validity may also change for flow immediately following the helium shock and subsequent helium flow due to boundary-layer growth.

Based on a static calibration of the transducer, the initial rise in the observed tube wall pressure was about 12 percent smaller than the free-stream pressure calculated from the helium shock velocity. The discrepancy could be reduced to about 8 percent by considering a probable attenuation of the helium shock in the acceleration chamber of the order of 2 percent. It was not possible to determine whether the remaining discrepancy resulted from a nonlinear behavior of the transducer or a real aerodynamic effect. (The pitot pressure transducer was statically calibrated but an error in calibration was discovered too late to recalibrate this transducer.)

Based on reference 7, an error of less than 3 percent is expected to be introduced in the pitot pressure measurements because of the change in Reynolds number as the flow changes from helium to nitrogen. Estimates of the unit Reynolds numbers are $5 \times 10^4/m$ for the helium flow and $2 \times 10^6/m$ for the nitrogen flow.

Shock and Interface Velocity

Intermediate chamber shock velocity.- The reported nitrogen shock velocity is the average velocity over the distance interval located approximately from 2.1 m to 0.4 m upstream of the secondary diaphragm. The estimated precision of these velocity measurements is of the order of ±0.5 percent.

Acceleration chamber shock velocity.- The reported helium shock velocity is the average velocity over the distance interval from the secondary diaphragm to the test section. The estimated precision of these velocity measurements is of the order of ±0.2 percent.

The possibility of a small attenuation of the helium shock velocity was indicated and is in agreement with the results reported in reference 1. The shock velocity was also measured over a distance interval of about 0.26 m located just upstream of the test section. The estimated precision for these measurements is of the order of ±3 percent. The shock velocities obtained in the vicinity of the test section averaged approximately 2 percent lower than the average velocities over the distance from the secondary diaphragm to the test section.

Interface velocity.- The reported helium-nitrogen interface velocity was measured for a distance interval of about 1.6 m located just upstream of the test section. The estimated precision of these measurements is of the order of ±0.8 percent.

An attenuation of the helium-nitrogen interface velocity was not indicated from the measurements. This result is in agreement with the results of reference 8, but not with the results of reference 1; however, the initial conditions (initial pressures) employed here are different than those employed for those two references. Microwave data from five tube runs were used to obtain the velocity for 12 equally spaced distance intervals located between the secondary diaphragm and the test section. The velocity obtained for the interval nearest the diaphragm was about 10 percent lower than the velocities obtained for the remaining distance intervals and was expected because of the initial acceleration of the interface as reported in reference 1. Except for the distance interval nearest the diaphragm, no change in interface velocity was observed to within an uncertainty of ±1 percent for the remaining distance to the test section.

Flow Velocity

The flow velocity u_m was obtained from:

$$u_m = \frac{x_2 - x_1}{t_{c,2} - t_{c,1}} = \frac{\Delta x}{\Delta t_c}$$

where x is the position of the center of the photodetector slit in the flow field, and t_c is the time when the geometric center of the luminous column coincides with the center of the photodetector slit. Shown in figure 7 are sample data oscillograms of the two photodetector signal pulses obtained during a velocity measurement. Values of $t_{c,1}$ and $t_{c,2}$ were obtained from these data.

Model of luminous column.- In order to relate the observed intensity at the photodetectors to spatial position of the luminous column, it was necessary to make at least three assumptions concerning the column: the column is symmetrical about its center of mass; the total emitted light decays with time; and the column increases in size with time.

As a result of light decay and column growth, the shape of the observed photodetector pulse is asymmetric. The time t_p at which peak intensity is observed is prior to t_c; that is,

$$t_p < t_c$$

Procedure.- The following procedure was used to analyze the data in obtaining values of t_c. Data from the oscillograms were reduced to numerical form for computation at time increments of 0.05 μsec. Corrections were applied to the data for the nonlinear response of the photodetectors and the decay of the light emitted by the column. Sample traces of corrected data pulses are shown in figure 8. Growth of the column can be inferred from a comparison of the two pulse widths.

The remaining asymmetry in the pulse shape was then assumed to be due to the growth of the column. The time t_c was taken to be the time for which one-half of the integrated pulse intensity had been observed.

Decay correction.- The correction for the decay of the emitted light consisted of the reciprocal of an empirically determined decay function. The decay function was derived from decay data obtained under static (no flow) conditions for nitrogen densities in the range of those encountered in the velocity measurements. The decay data indicated a complex decay of the emitted light following excitation of the column. However, the sum of two exponential functions approximated the decay during the time interval associated with detection of the column at the photodetector slits. The derived decay function used in correcting the data was

$$\frac{I}{I_0} = 0.9e^{-1.4t} + 0.1e^{-0.25t}$$

where t is the time in μsec following column excitation, I is the intensity at time t, and I_0 is the intensity at time $t = 0$.

Approximate size of column.- An initial column diameter of about 1.4 mm based on half-peak width was estimated from a photograph of the column obtained under static conditions in nitrogen. A short exposure time for the photograph was effected by means of a bandpass filter (3920 ± 40 Å), which primarily limited the exposure to rapidly decaying ($\approx 10^{-7}$ sec) light from the 0-0 band of excited N_2^+ ions. Shown in figure 9 is a scan of the intensity across the luminous column obtained by densitometry from the photograph. The location of the scan corresponds to the center line of the expansion tube. Also shown for the same location is the estimated diameter of the region illuminated by the ultraviolet light source.

Shown in figure 10 are the estimated diameters of the column as it passed the two photodetector slits. These estimates were obtained from the photodetector pulse widths and the flow velocity. The time is referenced to the time at which the column was produced. A radial velocity of the column boundary of about 150 m/sec can be inferred from the results shown in the figure. The observed rate of growth of the column is thought to be primarily due to heating of the column gas during excitation. The rate of growth due to ambipolar diffusion was estimated to be negligible compared with the observed rate.

Uncertainties.- Uncertainties associated with Δx and Δt_c lead to uncertainties in the flow velocity. The estimated uncertainties in the flow velocity are a random uncertainty of about ±1 percent for a single velocity measurement and a systematic uncertainty of about ±1 percent for all the velocity measurements. However, it should be recognized that the estimate of systematic uncertainty is based mainly on the assumed model of the luminous column. The same value of Δx was used in all the measurements. The estimated uncertainty in Δx is ±0.5 percent and introduces a systematic uncertainty of ±0.5 percent in all the velocity measurements. The nominal value of Δt_c was about 4.2 μsec. The estimated uncertainty in the time measurements of approximately ±1 percent introduces a random uncertainty in an individual velocity measurement of ±1 percent. A systematic error in Δt_c of up to 1 percent may be present as a result of errors in the assumed correction procedure. For example, it was assumed that the decay correction obtained under static conditions was applicable to the flow conditions. The correction procedure was expected to effect only a small correction to estimates of Δt_c which were based on uncorrected data, since the observed photodetector pulse shapes were close to being symmetrical. Estimates of Δt_c based on corrected and uncorrected data systematically differed by approximately 0.7 percent.

Derived Results

Shocked conditions.- The flow conditions following the passage of the helium and nitrogen shocks were derived from the initial conditions and the measured shock velocities. The relations used for computation were the adiabatic relations for a normal shock given in reference 6. Both helium and nitrogen were assumed to behave as perfect gases. The values used for γ were 5/3 for helium and 7/5 for nitrogen.

Density.- The flow density was derived from the measured flow velocity, pitot pressure, and tube wall pressure. The values of flow velocity, for times intermediate to those for which the velocity was measured, were obtained by linear interpolation between the measured values. For times greater than 600 μsec following the arrival of the helium shock, velocity values were obtained from a linear extrapolation of the trend of the measured velocity.

The density was computed by using the relation

$$\rho = \frac{p_t}{u^2}\left[\frac{M^2\gamma}{f(M^2,\gamma)}\right]$$

where $f(M^2,\gamma)$ is the supersonic pitot tube expression given in reference 5. For supersonic flow $\rho \approx \frac{p_t}{u^2}$, and the term in brackets was considered to be a correction term with a value close to unity. Approximate values for M were derived from the measured pitot pressures and tube wall pressures using the following approximation:

$$M^2 \approx M_a^2 \frac{M_a^2\gamma}{f(M_a^2,\gamma)}$$

where $M_a^2 = \frac{p_t}{\gamma p_w}$.

RESULTS AND DISCUSSION

Average values of the measured and derived results are presented in the figures and in tables II and III. The variances presented with the results indicate only the run-to-run reproducibility of the results. The symbol σ denotes the standard deviation from the mean value, and $\bar{\sigma}$ denotes the estimated variance of the mean value. The estimate used was $\bar{\sigma} = \sigma/\sqrt{n}$ where n is the number of expansion tube runs from which the mean value was obtained. The time is referenced to the start of flow at the test section. In this time frame, the helium shock arrived at $t = 0$, and the helium-nitrogen interface arrived at $t = 200 \pm 5$ μsec.

Predicted values from the idealized model are shown in some of the figures for comparison with the observed results. Initial conditions used for the model were the initial conditions in region (10) (fig. 1) and the conditions in region (2) derived from the measured nitrogen shock velocity. For computation, equations (1) and (2) and the normal shock relations given in reference 6 were used. The arrival time of the nitrogen shock at the second diaphragm was taken to be the same as that of the observed flow. For the model the helium shock arrived at the test section at $t = -360$ μsec and its arrival is not indicated in the figures; the helium-nitrogen interface arrived at $t = 275$ μsec, and the expansion fan arrived at $t = 725$ μsec.

Pitot Pressure

The observed trend of the pitot pressure is shown in figure 11. During the nitrogen flow, departure from a constant pressure is apparent. The large decrease in pressure in the interval from about 300 to 450 μsec is the pitot pressure dip described in reference 1. The minimum pressure of the dip is about 50 percent lower than the preceding peak pressure. During the 200 μsec of helium flow, a gradual increase in pitot pressure is indicated. The apparent lack of abrupt pressure changes associated with the arrival of the helium shock and helium-nitrogen interface is, at least partially, due to the filtering out of the higher frequency components of the pressure transducer signal.

The observed trend and magnitude of the pitot pressure are consistent with the results presented in reference 1, for which air instead of nitrogen was used as the test gas. The trends of pitot pressure, reported in figure 16 of reference 1, for differing initial conditions are shown in figure 12. For the initial conditions (figs. 12(a) and 12(b)), a pitot pressure dip is apparent, but is not apparent in the trends associated with conditions of figures 12(c) and 12(d). The initial conditions employed herein most closely correspond to the conditions shown in figure 12(a). The initial nitrogen pressure employed was about twice the initial air pressure employed for conditions of figure 12(a), which resulted in pitot pressure levels about twice those shown for conditions of figure 12(a). For the same initial pressures of nitrogen or air, the resultant pitot pressure levels are expected to be essentially the same.

Tube Wall Pressure

The observed trend of the tube wall pressure is shown in figure 13. During the nitrogen flow, departure from a constant pressure is apparent, but the relative pressure variations are smaller than is the case for the pitot pressure. Some points of similarity in the wall pressure and pitot pressure may be noted. However, the wall pressure peak and minimum occur earlier, and the minimum pressure is only 20 percent lower than the preceding peak pressure.

As was noted in reference 1, the wall pressure signal becomes noisy in the vicinity of the pitot pressure dip arrival. This can be seen in the sample data oscillogram shown in figure 6. The results shown in figure 13 do not reflect the noise oscillations, since these high-frequency oscillations were visually averaged in reducing the data oscillograms to numerical form. The time interval for which these oscillations occur is also shown in figure 13.

During the 200 μsec of helium flow, an increase in wall pressure is indicated. This trend is in agreement with the calculations of reference 9.

The wall pressure predicted by the model is larger than the observed pressure for the first 580 μsec of the real flow.

Flow Velocity

The trend of the observed flow velocity is indicated in figure 14. During the nitrogen flow, departure from a constant flow velocity is apparent, but the relative variation in velocity is smaller than the relative variations in the observed pressures. All the velocities in this time interval can be included within a range of 9 percent. A maximum in the observed flow velocity occurs during the passage of the pressure minimum of the pitot pressure dip. During the 160-μsec interval between the interface and the pressure minimum, the velocity increases by 2.5 percent. After the passage of the pressure minimum, the velocity decreases by 9 percent in the next 240 μsec.

An increase in flow velocity following the arrival of the interface is not unique to the operating condition for which a pitot pressure dip is observed. Larger increases in velocity (approximately 8 percent) were reported in reference 9 for operating conditions which differed significantly from the dip condition. For those conditions the higher velocities were observed within a 160-μsec interval following the interface, but locations of the maxima were not obtained. The value of p_1 was 0.5 of the value used here, and the values of p_{10} were about 0.05, 0.01, and 0.005 of the value employed.

The helium flow velocity immediately following the helium shock is also shown in figure 14. During the 200 μsec of helium flow, the increasing trend of the flow velocity (indicated in the figure by short dashed lines) was assumed since no velocity measurements were made in this interval. The relative values of flow velocity at the contact surface (measured) and flow velocity behind the shock (calculated) are in agreement with the ratios of the values determined in reference 9.

The velocity predicted by the model for the nitrogen flow is about 5 percent smaller than the velocities observed in the interval from the interface arrival time to 450 μsec. The predicted and observed velocities are in agreement late in the flow at 450, 500, and 600 μsec. The velocity predicted by the model for the helium flow is larger than the helium flow velocity immediately following the helium shock.

Derived Density

The density derived from the pitot pressure and flow velocity is shown in figure 15. The trend of the density is essentially the same as the trend of the pitot pressure, as might be expected from a consideration of the relatively small changes that occur in the flow velocity. The dip in pitot pressure corresponds to a dip in density as suggested in reference 1 and concluded in reference 8.

The density predicted from the idealized model is of the order of twice the derived density for the nitrogen flow. The predicted arrival of the interface approximately corresponds to the beginning of the pitot pressure dip.

Also shown in figure 15 is the nitrogen density which is predicted for an isentropic expansion from region (2) by using equation (1), the pressure and density in region (2), and the observed wall pressure at the test section. The derived density throughout the nitrogen flow interval is much less than the density obtained as the result of an isentropic process that may occur between region (2) and the test section. As inferred from the figure, the change in entropy is not constant over the nitrogen flow interval. A trend of decreasing entropy change for the flow interval following the density minimum is apparent. An extrapolation of this trend suggests that the expansion process may approach an isentropic process for $t > 1000$ μsec.

Since the nitrogen expansion process is not isentropic for this expansion tube operating condition, any flow models based solely on isentropic processes can not predict the derived density at the test section. This result confirms the suggestion made in reference 1 that a possible weak (isentropic) P-family expansion-wave interaction would probably not lead to an explanation of the pitot pressure dip or the low values of pitot pressure prior to the dip.

Based on the measurements reported herein, it is not possible to draw any conclusions concerning the possible mixing of the helium and nitrogen flows as suggested in reference 1. In the remaining presentation, it is assumed that no mixing of helium and nitrogen occurs for the observed flow.

Derived Flux

The timewise integral of the mass flux ρu reflects the lower density of the nitrogen flow as compared with the predictions of the idealized model and indicates a relative motion between the helium and nitrogen components of the observed flow. For the model, the integral from -360 μsec to 725 μsec is 65.8 g/m^2, which consists of 4.2 g/m^2 of helium and 61.6 g/m^2 of nitrogen. For the observed flow the integral from 0 μsec to 715 μsec is 37.8 g/m^2, which consists of 1.0 g/m^2 of helium and 36.8 g/m^2 of nitrogen. From comparison of the helium component for the two cases, it can be inferred for the

observed flow that the nitrogen near the interface has passed through about 76 percent of the helium that was initially located between the second diaphragm and the test section. The ratio of the helium to nitrogen components for the two cases is 0.068 for the model and 0.027 for the observed flow.

Derived Temperature

The temperature derived from the observed wall pressure and density by using the equation of state is shown in figure 16. A maximum in the observed temperature occurs at the same time as the minimum of the pitot pressure dip. The maximum temperature of the nitrogen is approximately the same as the temperature of the nitrogen in region ②. The predicted temperature is lower than the observed temperature throughout the nitrogen flow interval.

Run-to-Run Reproducibility

The reproducibility of several of the measured flow properties of the expansion tube cycle was examined. The measure used in this paper to infer or compare the reproducibility is the fractional variance from the mean (that is, σ/Mean value).

Helium-nitrogen interface velocity u_i.- Since the interface velocity was used to normalize the flow velocity measurements, it was of interest to see whether variations in u_i reflected variations in expansion tube operation. It was assumed that variations in nitrogen shock velocity $U_{s,1}$ reflected variations in the rupture of the primary diaphragm. For $n = 59$, the fractional variance of $U_{s,1}/u_i$ was ±1.0 percent, with corresponding variance for $U_{s,1}$ and u_i of ±2.2 percent and 1.9 percent. If the variations in u_i were assumed to be unrelated to the variations in $U_{s,1}$, the expected fractional variance of $U_{s,1}/u_i$ would be ±2.9 percent.

Measured flow velocity u_m.- Similar results were obtained for comparisons of the variations of u_i and the flow velocity u_m. For u_m corresponding to the peak and minimum of the pitot pressure, at $t = 275$ μsec and $t = 360$ μsec, $n = 7$. For these two time locations the fractional variances of u_m/u_i were ±1.2 percent and ±0.6 percent with corresponding variances for u_m and u_i of about ±2.3 percent and 2.2 percent. If the variations in u_m were assumed to be unrelated to the variations in u_i, the expected fractional variance of u_m/u_i would be about ±3.2 percent.

Flow velocity, wall pressure, and pitot pressure u, p_w, p_t.- The fractional variances of three properties measured at the test section are shown in figure 17. Listed in order from the most to the least reproducible, the properties are (1) the flow velocity, (2) the tube wall pressure, and (3) the pitot pressure.

Significant increases in the fractional variances occur in the interval of the pitot pressure dip for the three properties. The increases occur in the vicinity of the minimum of the pitot pressure dip for the flow velocity and pitot pressure, which were observed at the center line of the expansion tube, but occurs near the onset of the dip for the tube wall pressure. A significant decrease in the fractional variance occurs at approximately $t = 520$ μsec for the pitot pressure, but no significant changes are apparent in this vicinity for the two other properties.

Integrated flux.- In practice, the definite integral of a property over a reasonably finite time interval is often of more interest than the distribution of that property within the time interval, particularly, for an impulse facility such as an expansion tube. The fractional variance of the definite integral of the mass flux is shown in figure 18 for several time intervals. The variance of the derived flux ρu reflects only the variance of the pitot pressure which is shown again for comparison. The relatively smaller variance of the velocity was not considered in obtaining the variance of the flux. Although a rather large variance for the flux can be expected for an arbitrary time during the nitrogen flow, the integral of the flux for a time interval of 500 μsec can be expected to be reproducible to within about ±3 percent.

SUMMARY OF RESULTS

Measurements of flow velocity, pitot pressure, and tube wall pressure were made employing a single expansion tube operating condition, for which a significant decrease or dip in pitot pressure occurs during the test flow time interval. Supplemental to the three properties measured at the test section were measurements of the intermediate chamber shock velocity, the acceleration chamber shock velocity, and the helium-nitrogen interface velocity. The following characteristics of the test flow and expansion tube flow cycle were derived from these measurements.

Main Results

The main results are as follows:

1. The variations which occur during the test flow time interval in flow velocity and tube wall pressure are small relative to the variations in pitot pressure.

2. In the time interval in which the pitot pressure dip is observed, a corresponding dip in the derived flow density occurs.

3. With regard to the overall expansion processes which occur between the shocked conditions of the test gas in the intermediate chamber and the conditions at the test section, a larger expansion occurs than can result from only isentropic processes.

Specifically, the value of the average density over the observed nitrogen flow interval is about one-half the value that would result from an isentropic expansion to the observed pressure. This result is consistent with the lower than expected levels of pitot pressure reported in NASA TN D-3421.

Specific Results

The specific results are as follows:

1. The interface velocity measured by means of microwave agrees with the flow velocity measured 30 μsec following passage of the interface to within an uncertainty of about ±1 percent.

2. Following the passage of the interface, the flow velocity increases to a maximum value 2.5 percent larger than the interface velocity during 160 μsec of flow, and then decreases to a value about 6.5 percent smaller than the interface velocity during the next 240 μsec.

3. The maximum in the flow velocity occurs at a time which coincides with the passage of the minimum pressure of the pitot pressure dip.

4. Small variations in the intermediate chamber shock velocity are reflected in the interface velocity measured at the test section.

5. Small variations in the interface velocity are reflected in the nitrogen flow velocity in the interval from interface arrival to arrival of the minimum pressure of the pitot pressure dip, but may be reflected to a lesser degree for subsequent time intervals.

6. Of the three properties measured at the test section within the nitrogen flow interval, the most reproducible property was the flow velocity; next was the tube wall pressure; and the least reproducible was the pitot pressure.

7. An increase in the fractional variance of the tube wall pressure occurred near the onset of the pitot pressure dip, whereas increases in the fractional variances of the pitot pressure and the flow velocity occurred nearer the minimum pressure of the pitot pressure dip.

8. The timewise integral of the mass flux over the 515 μsec nitrogen flow interval was reproducible to within about ±3 percent.

Langley Research Center,
National Aeronautics and Space Administration,
Hampton, Va., June 3, 1974.

REFERENCES

1. Jones, Jim J.; and Moore, John A.: Exploratory Study of Performance of the Langley Pilot Model Expansion Tube With a Hydrogen Driver. NASA TN D-3421, 1966.

2. Trimpi, Robert L.: A Preliminary Theoretical Study of the Expansion Tube, a New Device for Producing High-Enthalpy Short-Duration Hypersonic Gas Flows. NASA TR R-133, 1962.

3. Gartrell, Luther R.: A Technique for Measuring Hypersonic Flow Velocity Profiles. NASA TN D-7270, 1973.

4. Duckett, Roy J.; and Sebacher, Daniel I.: Velocity Measurements in the Langley 1-Foot (0.305-Meter) Hypersonic Arc Tunnel. NASA TN D-3308, 1966.

5. Friesen, Wilfred J.: Use of Photoionization in Measuring Velocity Profile of Free-Stream Flow in Langley Pilot Model Expansion Tube. NASA TN D-4936, 1968.

6. Mueller, James N.: Equations, Tables, and Figures for Use in the Analysis of Helium Flow at Supersonic and Hypersonic Speeds. NACA TN 4063, 1957.

7. Bailey, A. B.; and Boylan, D. E.: Some Experiments on Impact-Pressure Probes in a Low-Density, Hypervelocity Flow. AEDC-TN-61-161, U.S. Air Force, Dec. 1961.

8. Haggard, Kenneth V.: Free-Stream Temperature, Density, and Pressure Measurements in an Expansion Tube Flow. NASA TN D-7273, 1973.

9. Mirels, H.: Flow Nonuniformity in Shock Tubes Operating at Maximum Test Times. Phys. Fluids, vol. 9, no. 10, Oct. 1966, pp. 1907-1912.

TABLE I.- INITIAL CONDITIONS

[Expansion tube diameter, 9.55 cm]

Chamber	Length, m	Filling gas	Pressure, kN/m^2	Temperature, K
Driver	1.61	Hydrogen	8300	297
Intermediate	10.97	Nitrogen	6.67	297
Acceleration	9.72	Helium	0.267	297

TABLE II.- MEASURED RESULTS

(a) Pitot pressure; n = 4

t, μsec	p_t, kN/m^2	$\bar{\sigma}$, kN/m^2
0	----	----
5	7.9	±0.7
10	12.2	.6
15	15.1	.7
20	16.9	.6
25	18.1	.6
30	19.1	.6
35	20.0	.7
40	20.6	.8
45	21.2	.8
50	21.5	.7
55	22.0	.7
60	22.3	.6
65	22.5	.6
70	22.7	.7
75	23.1	.7
80	23.4	.7
85	23.6	.8
90	23.6	.8
95	23.7	.8
100	23.9	.8
105	24.1	.8
110	24.3	.7
115	24.5	.7
120	24.6	.6
125	24.7	.6
130	24.9	.6
135	25.0	.5
140	25.0	.5
145	25.1	.6
150	25.3	.6
155	25.4	.7
160	25.4	.7
165	25.5	.7
170	25.5	.6
175	25.5	.7
180	25.5	.7
185	25.5	.7
190	25.6	.6
195	26.3	.6
200	30.3	2.4
205	40.6	2.3
210	57.7	3.2
215	96.7	3.2
220	173	10
225	221	8
230	245	10
235	266	9
240	292	7
245	314	6
250	329	±5
255	331	6
260	330	7
265	332	9
270	331	11
275	329	13
280	330	12
285	332	12
290	317	14
295	301	15
300	285	16
305	255	18
310	237	15
315	227	11
320	215	5
325	206	4
330	207	4
335	210	15
340	212	17
345	215	11
350	194	13
355	184	10
360	186	14
365	181	22
370	181	19
375	185	13
380	200	26
385	238	23
390	258	24
395	243	26
400	249	32
405	251	29
410	241	20
415	247	25
420	244	20
425	234	10
430	227	26
435	222	23
440	217	26
445	254	30
450	295	28
455	297	20
460	307	15
465	322	11
470	328	18
475	317	23
480	303	21
485	281	20
490	279	33
495	283	33
500	297	±23
505	300	24
510	291	24
515	288	24
520	291	17
525	309	6
530	317	10
535	302	11
540	307	11
545	320	13
550	312	10
555	298	12
560	282	10
565	289	14
570	294	17
575	295	11
580	305	11
585	309	9
590	311	13
595	310	10
600	309	6
605	306	7
610	308	6
615	318	3
620	330	7
625	329	13
630	328	12
635	322	3
640	313	8
645	320	7
650	347	20
655	351	19
660	354	10
665	351	12
670	350	10
675	356	10
680	352	14
685	363	12
690	382	14
695	389	11
700	382	8
705	377	4
710	377	9
715	364	10

TABLE II.- MEASURED RESULTS - Continued

(b) Tube wall pressure; n = 4

t, μsec	p_w, kN/m^2	$\bar{\sigma}$, kN/m^2
0	----	----
5	7.31	±0.13
10	7.54	.12
15	7.76	.11
20	7.95	.12
25	8.16	.13
30	8.38	.12
35	8.57	.12
40	8.77	.12
45	8.96	.12
50	9.14	.13
55	9.28	.13
60	9.40	.14
65	9.45	.13
70	9.43	.12
75	9.38	.11
80	9.30	.10
85	9.21	.09
90	9.16	.08
95	9.12	.08
100	9.09	.09
105	9.08	.10
110	9.10	.09
115	9.14	.09
120	9.20	.08
125	9.29	.08
130	9.42	.09
135	9.52	.13
140	9.62	.17
145	9.64	.16
150	9.63	.14
155	9.70	.10
160	9.75	.08
165	9.72	.08
170	9.64	.12
175	9.50	.13
180	9.30	.11
185	9.06	.05
190	8.89	.05
195	8.80	.06
200	8.79	.08
205	8.83	.09
210	8.94	.12
215	9.07	.12
220	9.19	.11
225	9.34	.09
230	9.45	.09
235	9.52	.10
240	9.54	.15
245	9.54	.20
250	9.47	±0.20
255	9.18	.15
260	9.08	.16
265	8.96	.13
270	8.77	.11
275	8.52	.18
280	8.26	.27
285	8.06	.29
290	7.83	.25
295	7.75	.18
300	7.83	.14
305	8.15	.11
310	8.43	.10
315	8.65	.10
320	8.74	.16
325	8.65	.24
330	8.58	.24
335	8.50	.18
340	8.49	.19
345	8.37	.27
350	8.27	.34
355	8.25	.32
360	8.23	.23
365	8.26	.17
370	8.38	.13
375	8.51	.08
380	8.62	.10
385	8.69	.13
390	8.79	.15
395	8.89	.17
400	8.97	.20
405	9.05	.22
410	9.12	.25
415	9.23	.26
420	9.39	.24
425	9.56	.25
430	9.65	.27
435	9.66	.29
440	9.71	.30
445	9.84	.26
450	9.76	.26
455	9.75	.30
460	9.84	.22
465	9.89	.10
470	9.82	.09
475	9.74	.14
480	9.73	.21
485	9.82	.22
490	9.79	.27
495	9.75	.32
500	9.80	±0.26
505	9.92	.25
510	10.07	.26
515	10.20	.30
520	10.25	.35
525	10.27	.34
530	10.31	.24
535	10.21	.20
540	10.05	.20
545	10.03	.20
550	10.08	.22
555	10.08	.24
560	10.17	.27
565	10.36	.26
570	10.51	.28
575	10.70	.30
580	10.96	.31
585	11.17	.31
590	11.20	.33
595	11.08	.31
600	10.91	.29
605	10.77	.27
610	10.70	.26
615	10.66	.26
620	10.64	.28
625	10.65	.31
630	10.66	.33
635	10.73	.27
640	10.81	.20
645	10.87	.14
650	10.94	.16
655	11.04	.21
660	11.21	.23
665	11.39	.25
670	11.56	.25
675	11.65	.28
680	11.69	.31
685	11.67	.35
690	11.61	.39
695	11.59	.41
700	11.54	.37
705	11.45	.31
710	11.40	.22
715	11.49	.16

TABLE II.- MEASURED RESULTS - Concluded

(c) Boundary velocities; n = 4

Boundary	Velocity, m/sec	$\bar{\sigma}$, m/sec
Nitrogen shock	2406	±6
Helium shock	4731	12
He-N_2 interface	4376	18

(d) Flow velocity

t, μsec	u, m/sec	$\bar{\sigma}$, m/sec	n
230	4376	±20	3
275	4437	21	7
360	4485	10	7
400	4293	60	3
450	4179	70	2
500	4197	77	2
600	4092	96	2

TABLE III.- DERIVED RESULTS

(a) Conditions following nitrogen shock derived from initial conditions and shock velocity

u_2, m/sec	1960
a_2, m/sec	1110
p_2, kN/m^2	364
ρ_2, g/m^3	410
T_2, K	2990

(b) Conditions following helium shock derived from initial conditions and shock velocity

u_{20}, m/sec	3390
a_{20}, m/sec	2810
p_{20}, kN/m^2	7.20
ρ_{20}, g/m^3	1.52
T_{20}, K	2280

TABLE III.- DERIVED RESULTS - Concluded

(c) Flow density derived from pitot pressure, tube wall pressure, and flow velocity; n = 4

t, μsec	ρ, g/m³	$\bar{\sigma}$, g/m³
0	----	----
5	0.29	±0.07
10	.75	.05
15	1.03	.06
20	1.17	.06
25	1.26	.05
30	1.33	.05
35	1.38	.06
40	1.40	.07
45	1.43	.07
50	1.43	.06
55	1.44	.06
60	1.45	.05
65	1.45	.06
70	1.44	.06
75	1.46	.05
80	1.47	.06
85	1.47	.06
90	1.45	.06
95	1.44	.06
100	1.44	.06
105	1.44	.05
110	1.43	.05
115	1.43	.05
120	1.42	.04
125	1.41	.04
130	1.40	.04
135	1.38	.04
140	1.36	.03
145	1.35	.04
150	1.35	.04
155	1.34	.04
160	1.32	.04
165	1.31	.04
170	1.30	.04
175	1.29	.04
180	1.28	.04
185	1.28	.04
190	1.28	.04
195	1.31	.04
200	1.53	.15
205	2.06	.13
210	3.03	.18
215	5.25	.18
220	9.58	.5
225	12.3	.5
230	13.7	.5
235	14.8	.5
240	16.2	.4
245	17.4	.4
250	18.2	±0.3
255	18.3	.3
260	18.2	.4
265	18.2	.5
270	18.1	.6
275	18.0	.7
280	18.0	.6
285	18.1	.6
290	17.3	.8
295	16.4	.8
300	15.4	.9
305	13.8	1.0
310	12.7	.8
315	12.2	.6
320	11.5	.3
325	11.0	.2
330	11.1	.2
335	11.2	.8
340	11.3	.9
345	11.5	.6
350	10.3	.7
355	9.8	.5
360	9.8	.7
365	9.7	1.2
370	9.8	1.1
375	10.1	.7
380	11.1	1.5
385	13.3	1.3
390	14.6	1.4
395	13.9	1.5
400	14.4	1.9
405	14.7	1.7
410	14.1	1.2
415	14.5	1.5
420	14.5	1.2
425	13.9	.6
430	13.6	1.6
435	13.3	1.4
440	13.1	1.7
445	15.4	1.8
450	18.1	1.8
455	18.2	1.2
460	18.8	.9
465	19.7	.7
470	20.0	1.1
475	19.4	1.4
480	18.5	1.3
485	17.1	1.3
490	17.0	2.0
495	17.2	2.1
500	18.1	±1.4
505	18.3	1.5
510	17.8	1.5
515	17.6	1.5
520	17.8	1.2
525	19.0	.4
530	19.6	.6
535	18.7	.7
540	19.1	.7
545	19.9	.8
550	19.5	.7
555	18.6	.8
560	17.6	.7
565	18.1	.9
570	18.5	1.1
575	18.6	.7
580	19.3	.7
585	19.6	.6
590	19.7	.9
595	19.7	.6
600	19.7	.4
605	19.6	.5
610	19.8	.4
615	20.5	.2
620	21.3	.5
625	21.3	.8
630	21.2	.8
635	20.9	1.5
640	20.4	.6
645	20.8	.4
650	22.7	1.4
655	23.0	1.3
660	23.2	.7
665	23.1	.8
670	23.1	.7
675	23.6	.7
680	23.3	.8
685	24.1	.8
690	25.5	.9
695	26.0	.8
700	25.6	.6
705	25.3	.3
710	25.3	.6
715	24.5	.7

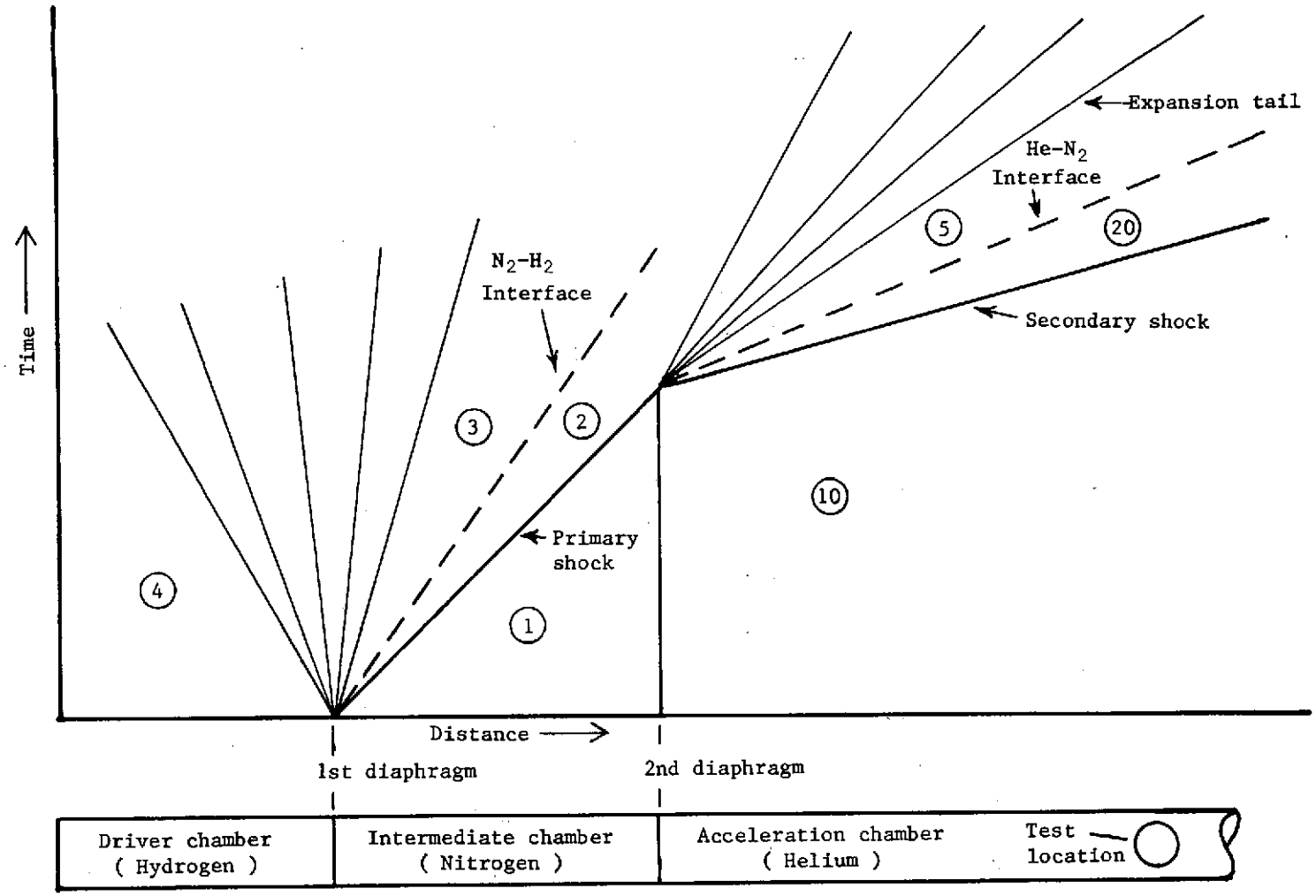

Figure 1.- Distance-time diagram of an idealized expansion tube flow cycle showing pertinent flow regions.

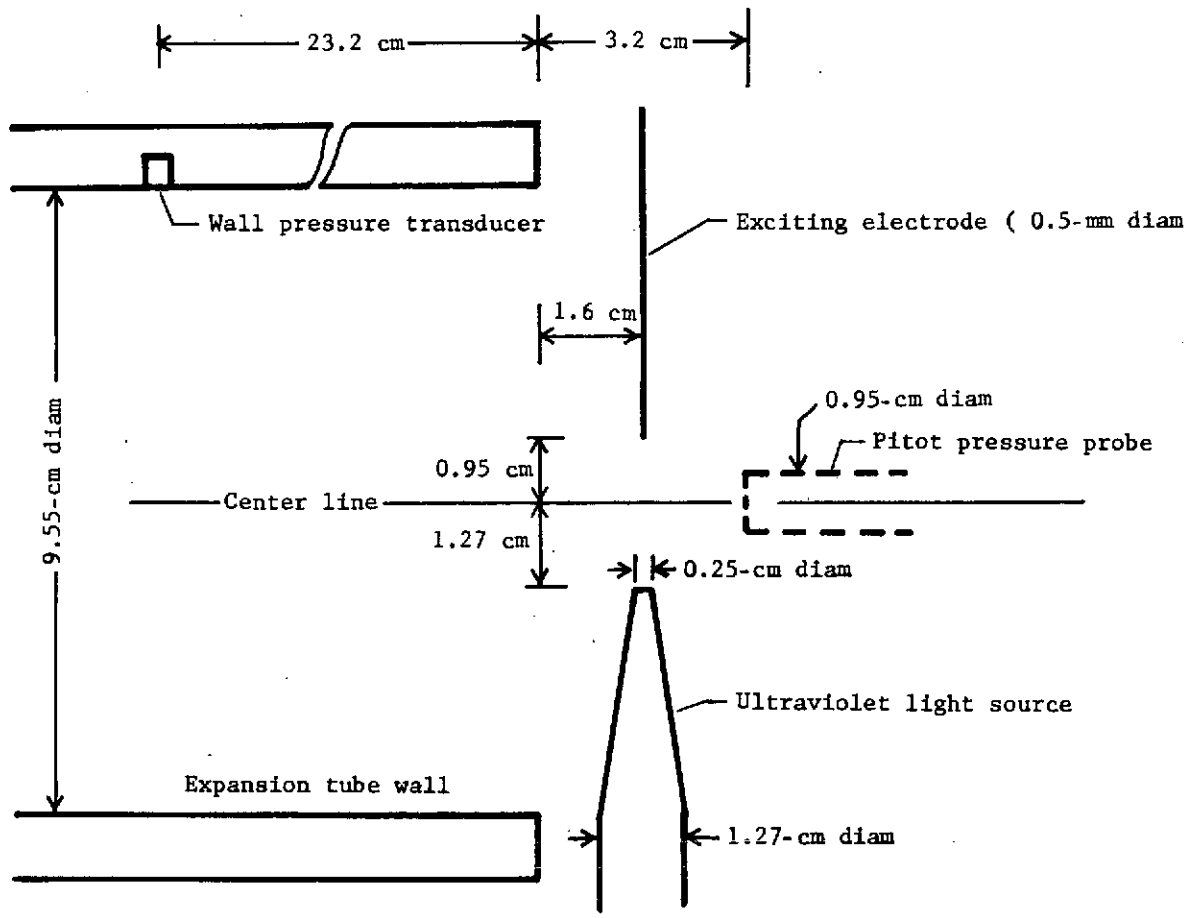

Figure 2.- Arrangement of components at expansion tube test section. Side view.

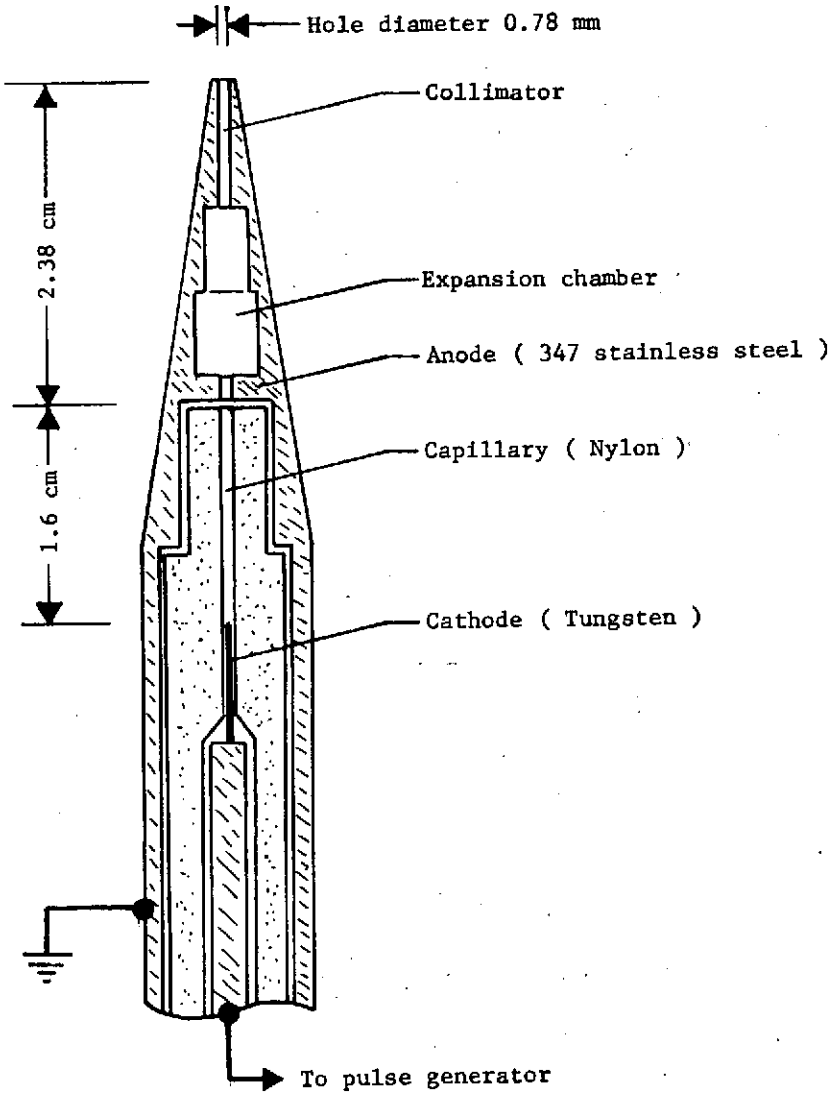

Figure 3.- Sketch of windowless ultraviolet light source.

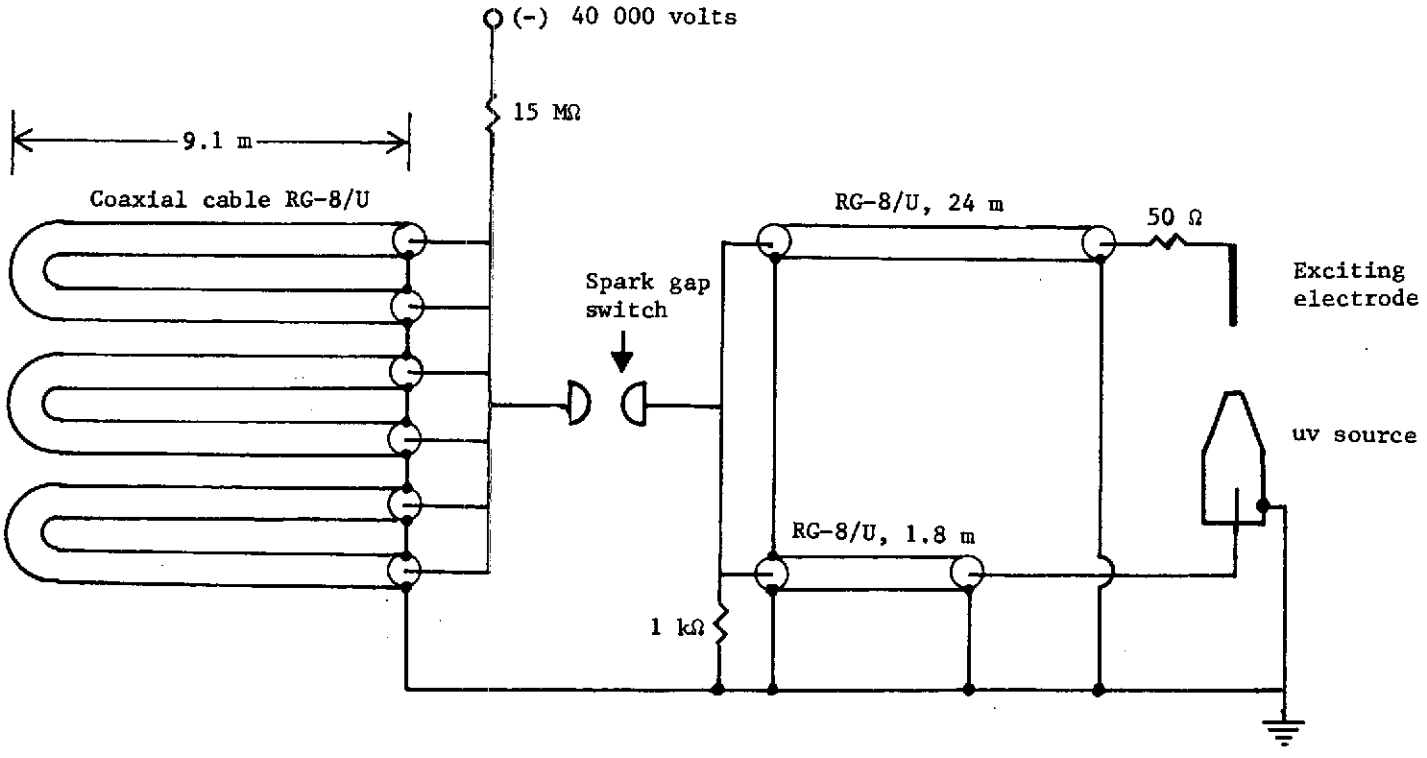

Figure 4.- Circuit diagram of pulse generator.

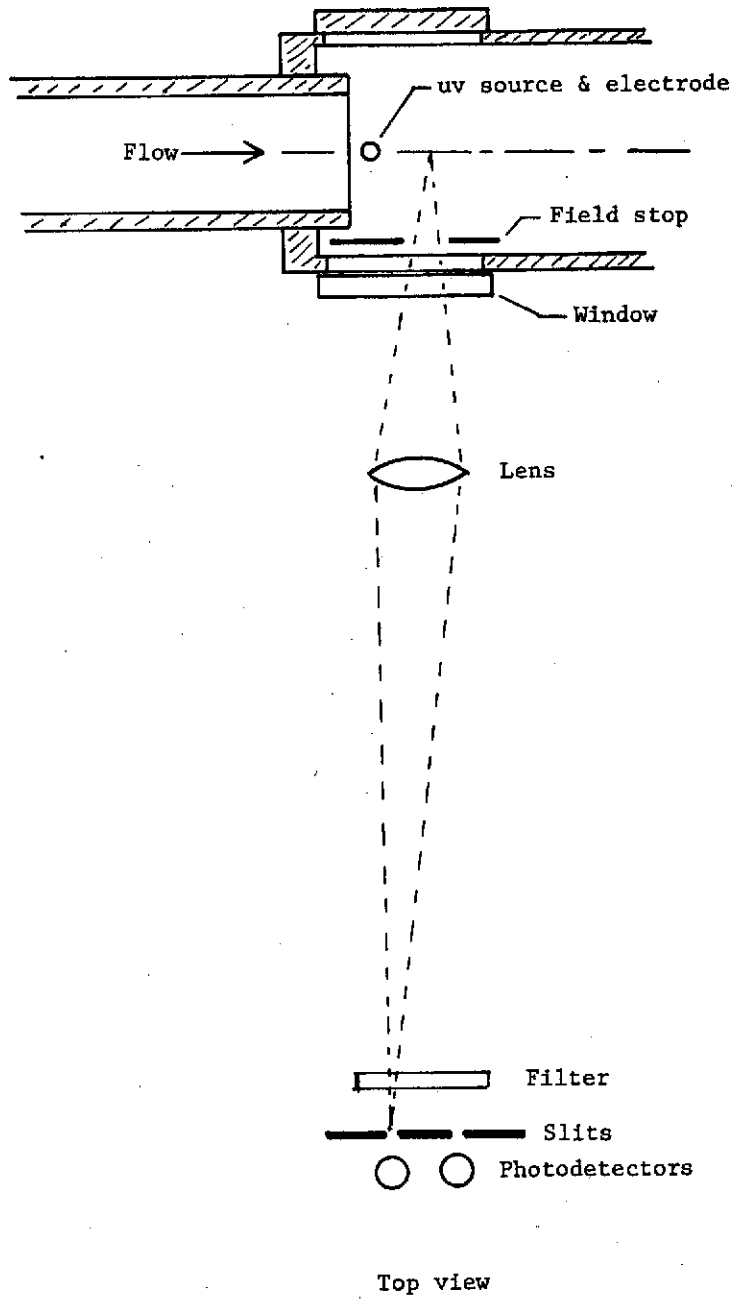

Figure 5.- Sketch of optical arrangement.

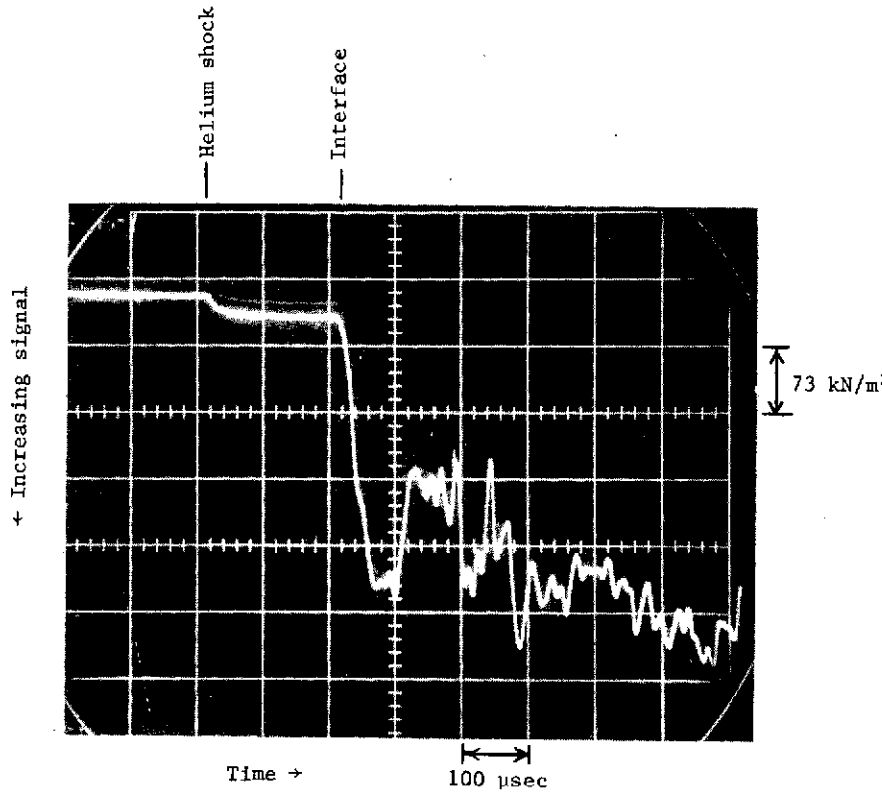

(a) Pitot pressure.

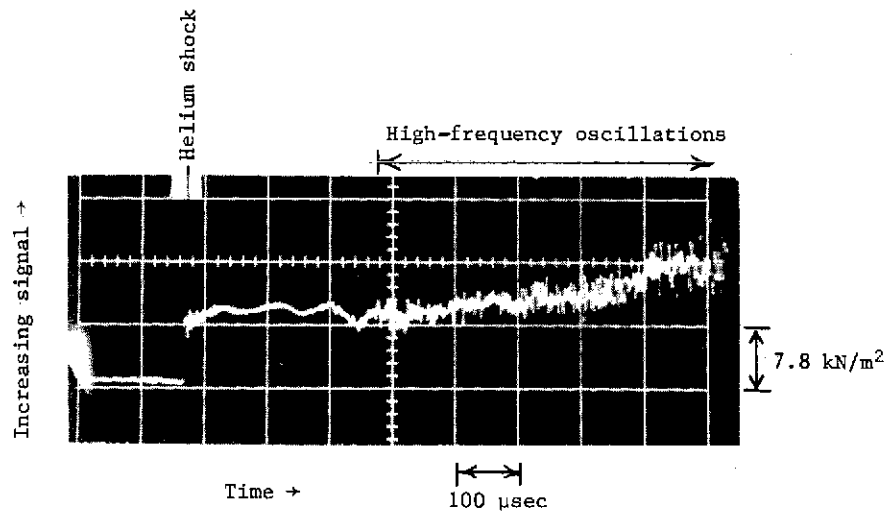

(b) Tube wall pressure.

Figure 6.- Sample data oscillograms of pitot and tube wall pressure gage signals.

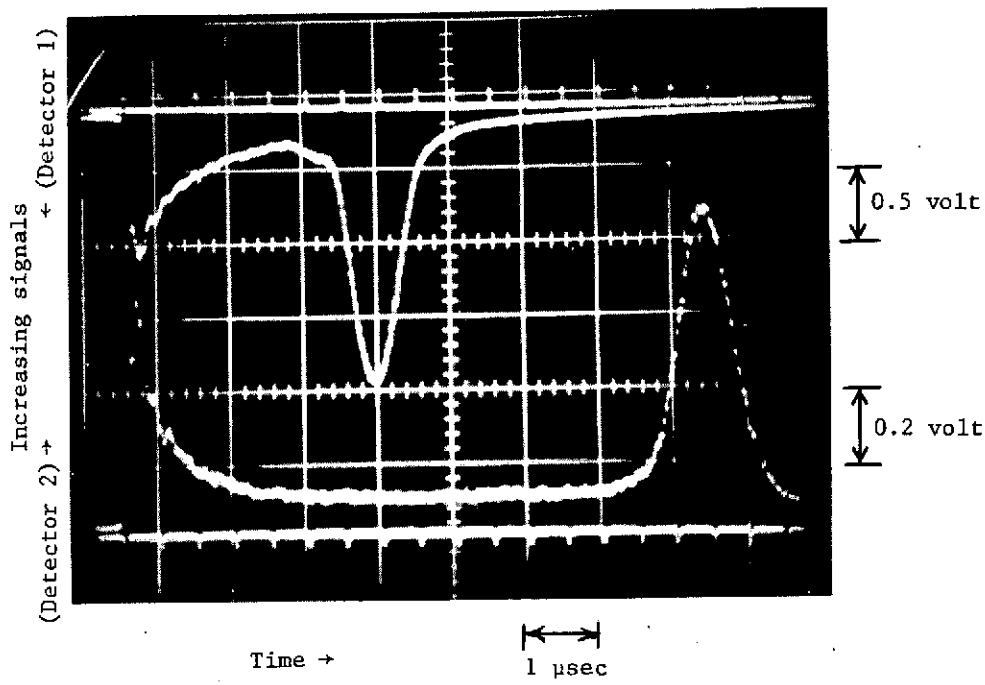

Figure 7.- Sample data oscillograms of photodetector signals.

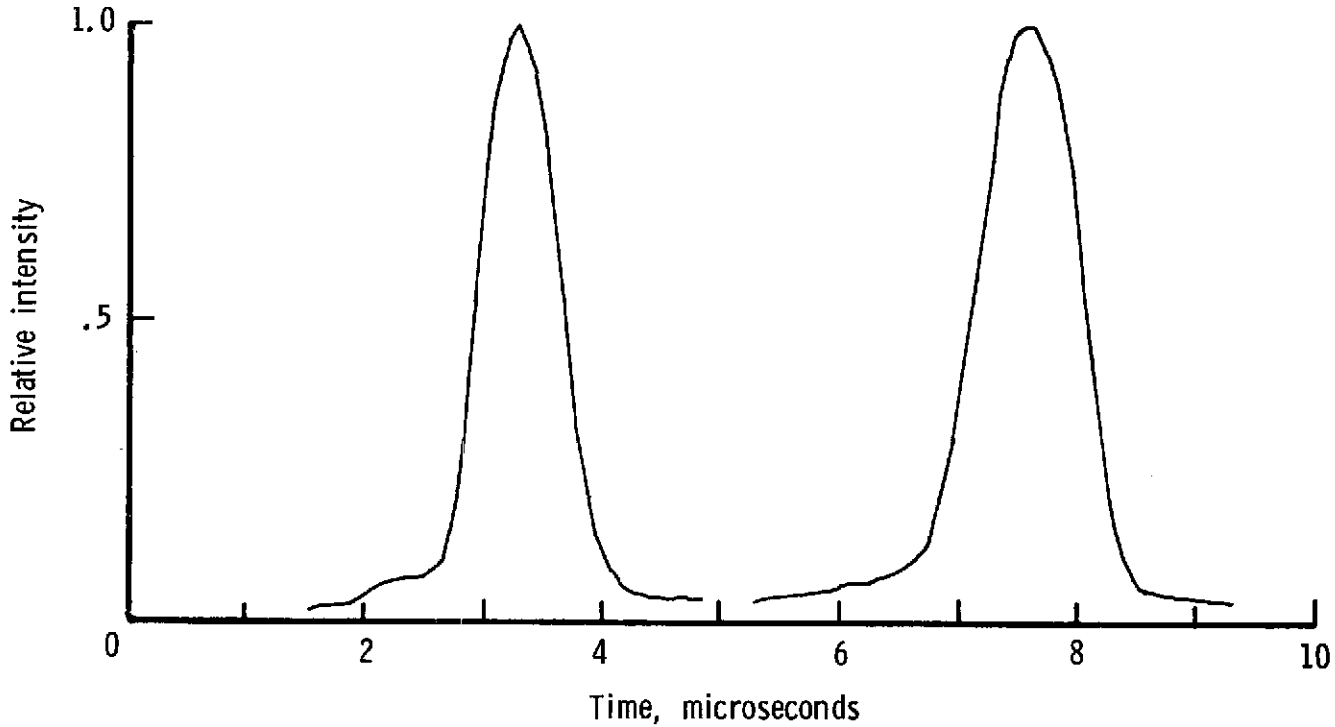

Figure 8.- Sample photodetector signals corrected for nonlinear response and light decay.

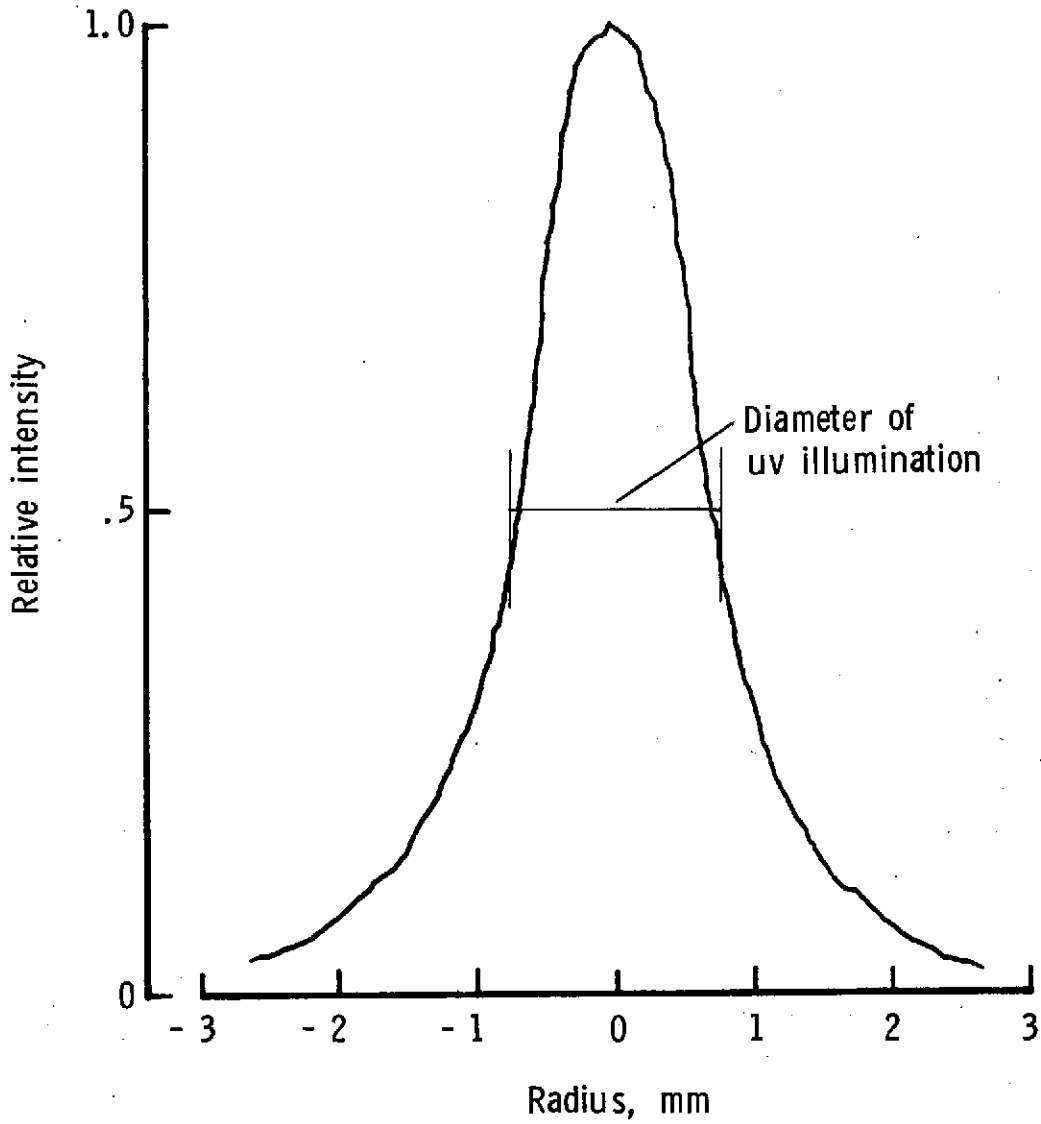

Figure 9.- Intensity scan of luminous column at expansion tube center line, approximately 0.2 μsec after excitation. No flow.

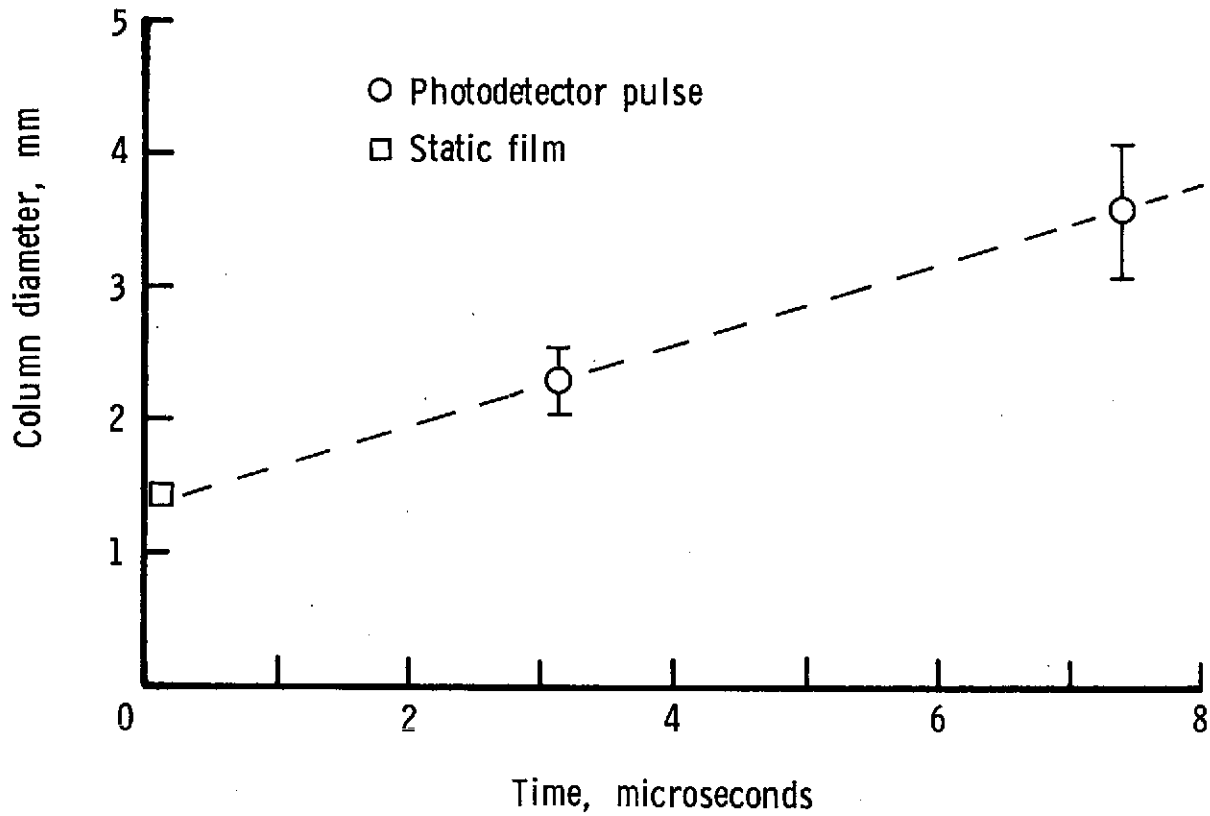

Figure 10.- Estimated diameter of luminous column at the photodetector slit positions. Time is referenced to the excitation of the column.

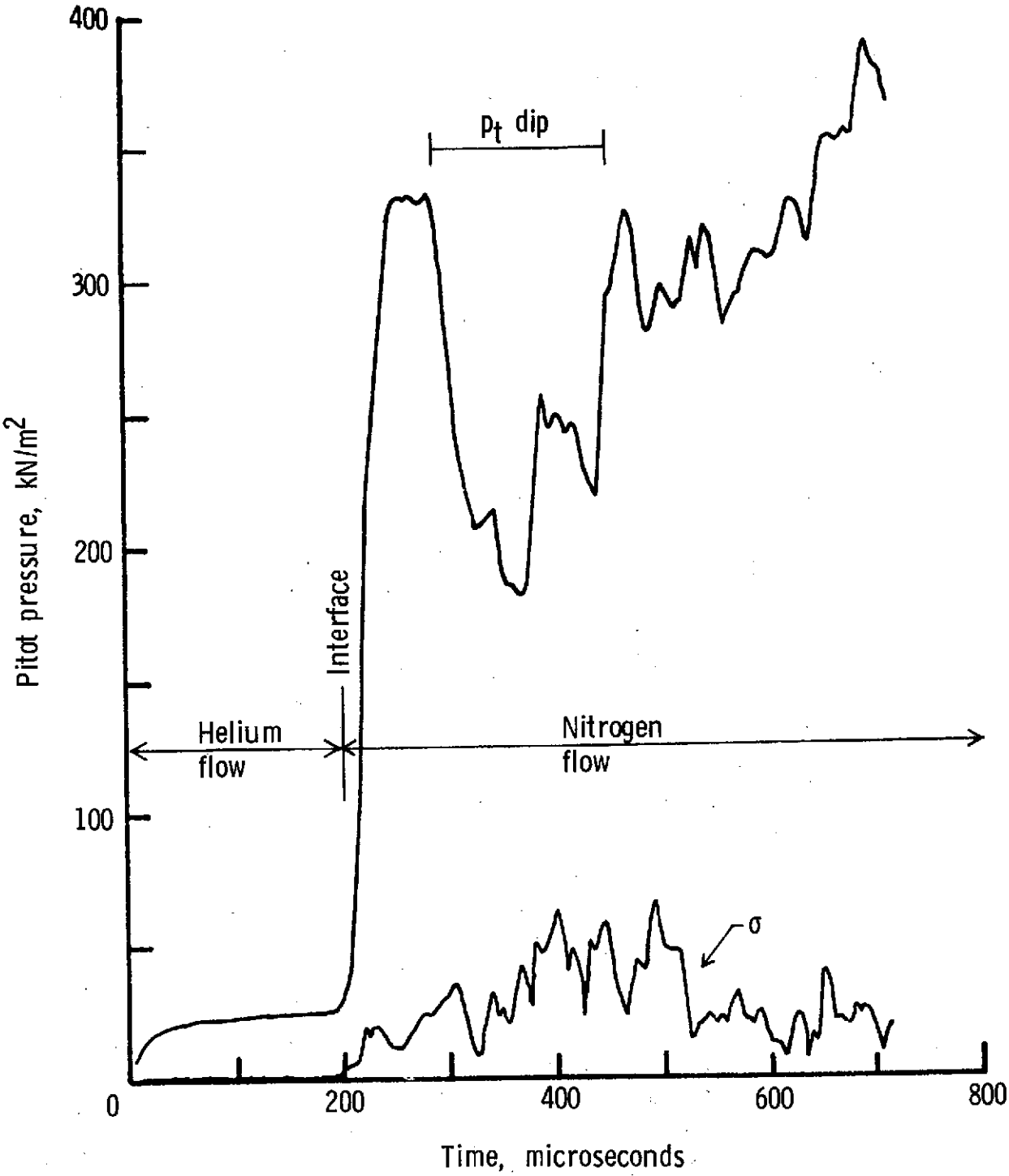

Figure 11.- Pitot pressure.

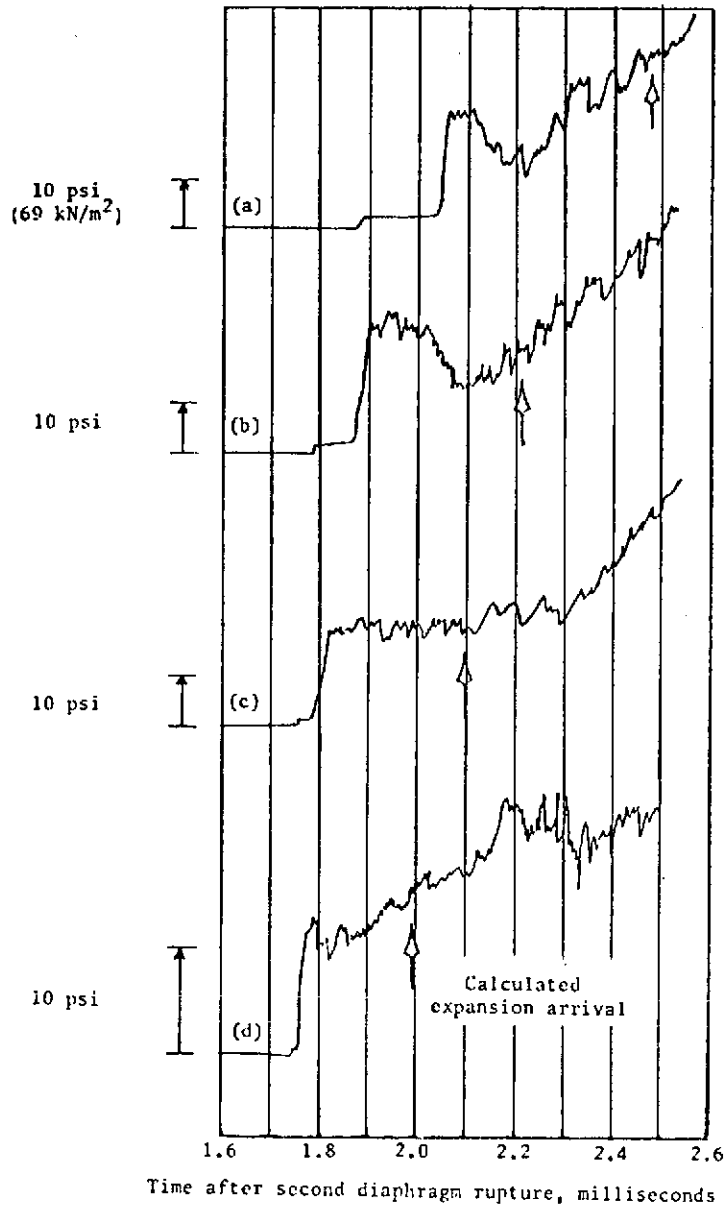

(a) p_{10} = 1.98 torr = 264 N/m^2.
(b) p_{10} = 0.95 torr = 127 N/m^2.
(c) p_{10} = 0.45 torr = 60.0 N/m^2.
(d) p_{10} = 0.095 torr = 12.7 N/m^2.

Figure 12.- Pitot pressure tracings showing effect of varying acceleration-chamber pressure p_{10}. (Reproduction of fig. 16, ref. 1.)

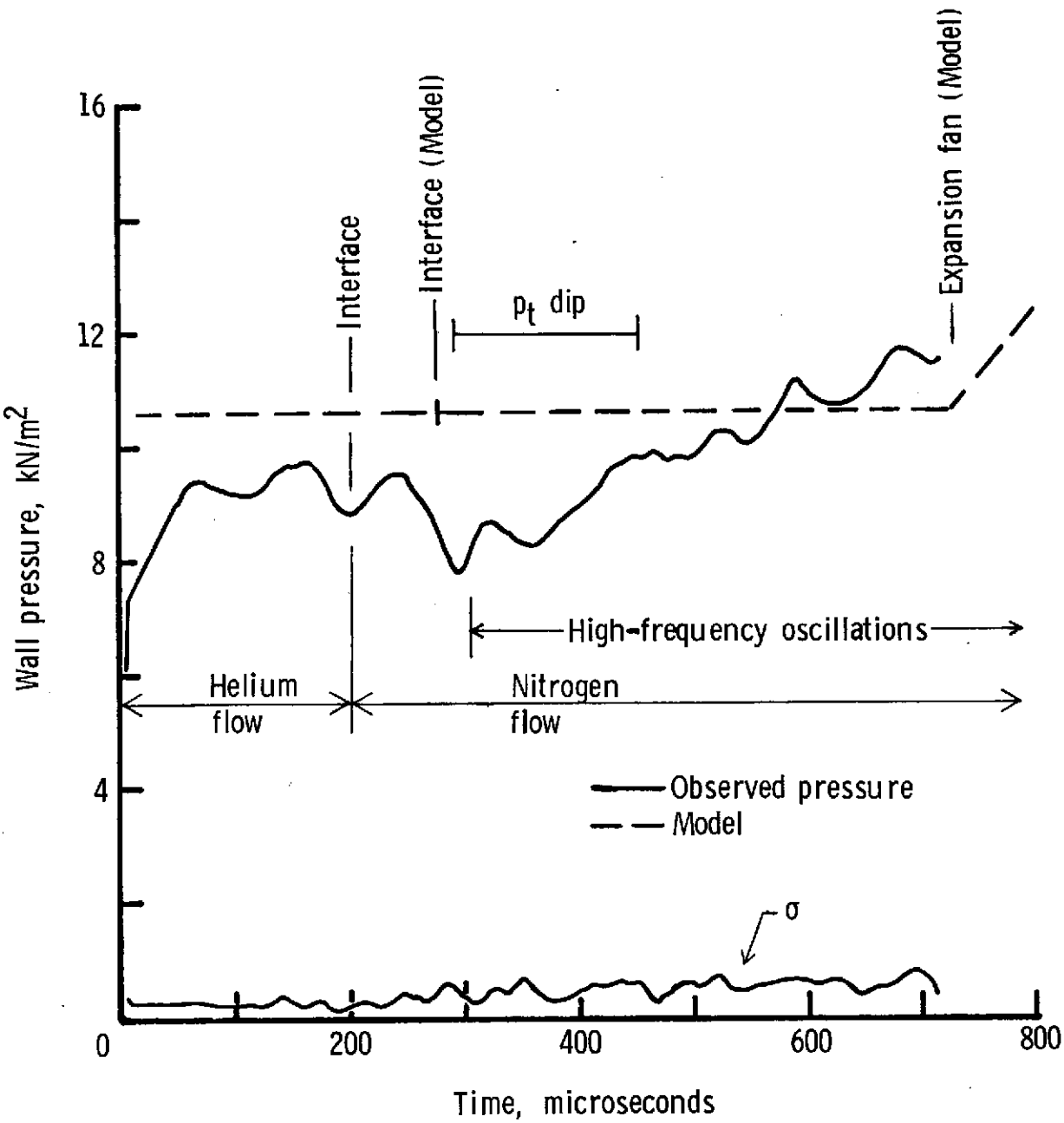

Figure 13.- Tube wall pressure.

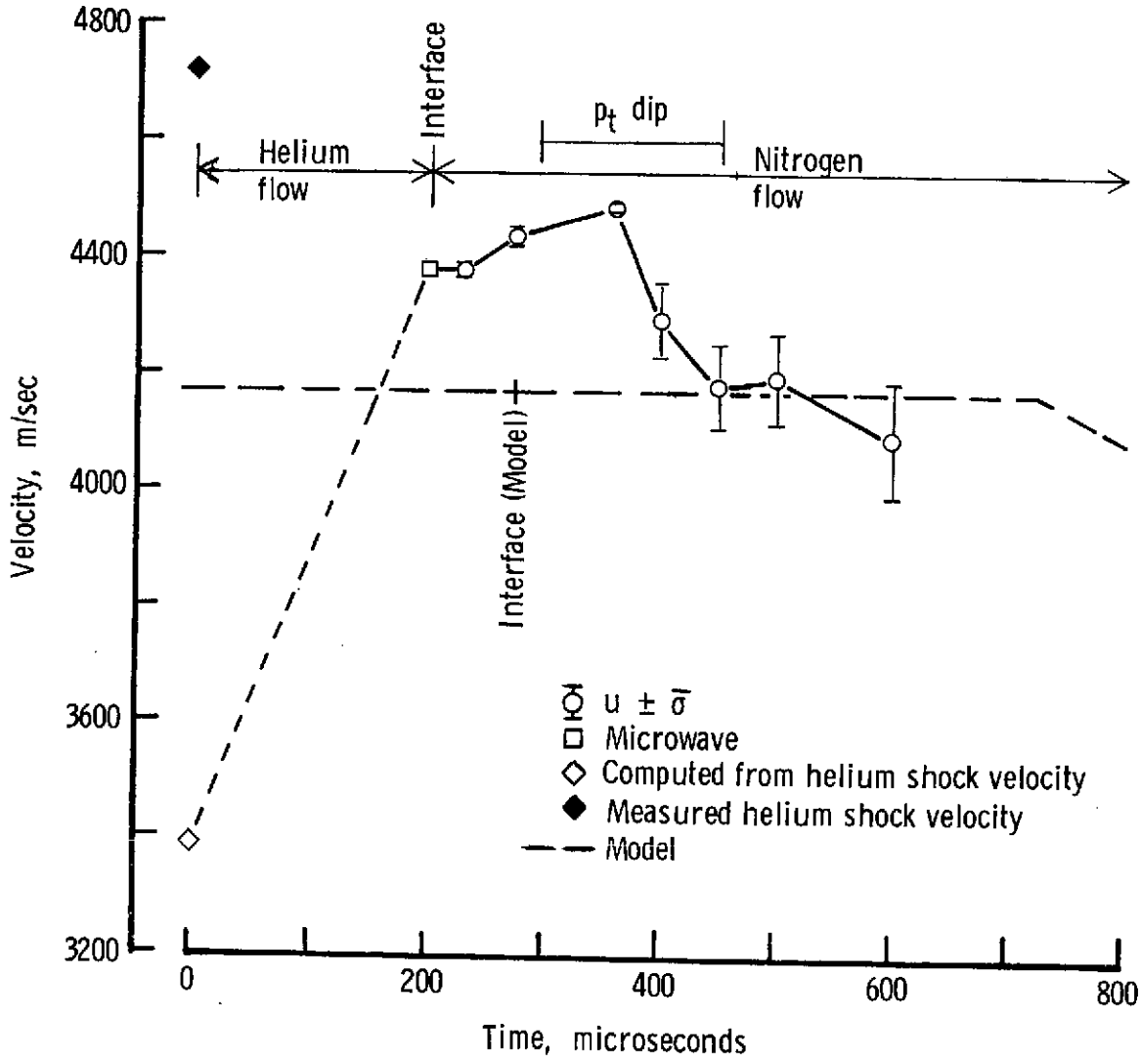

Figure 14.- Flow velocity.

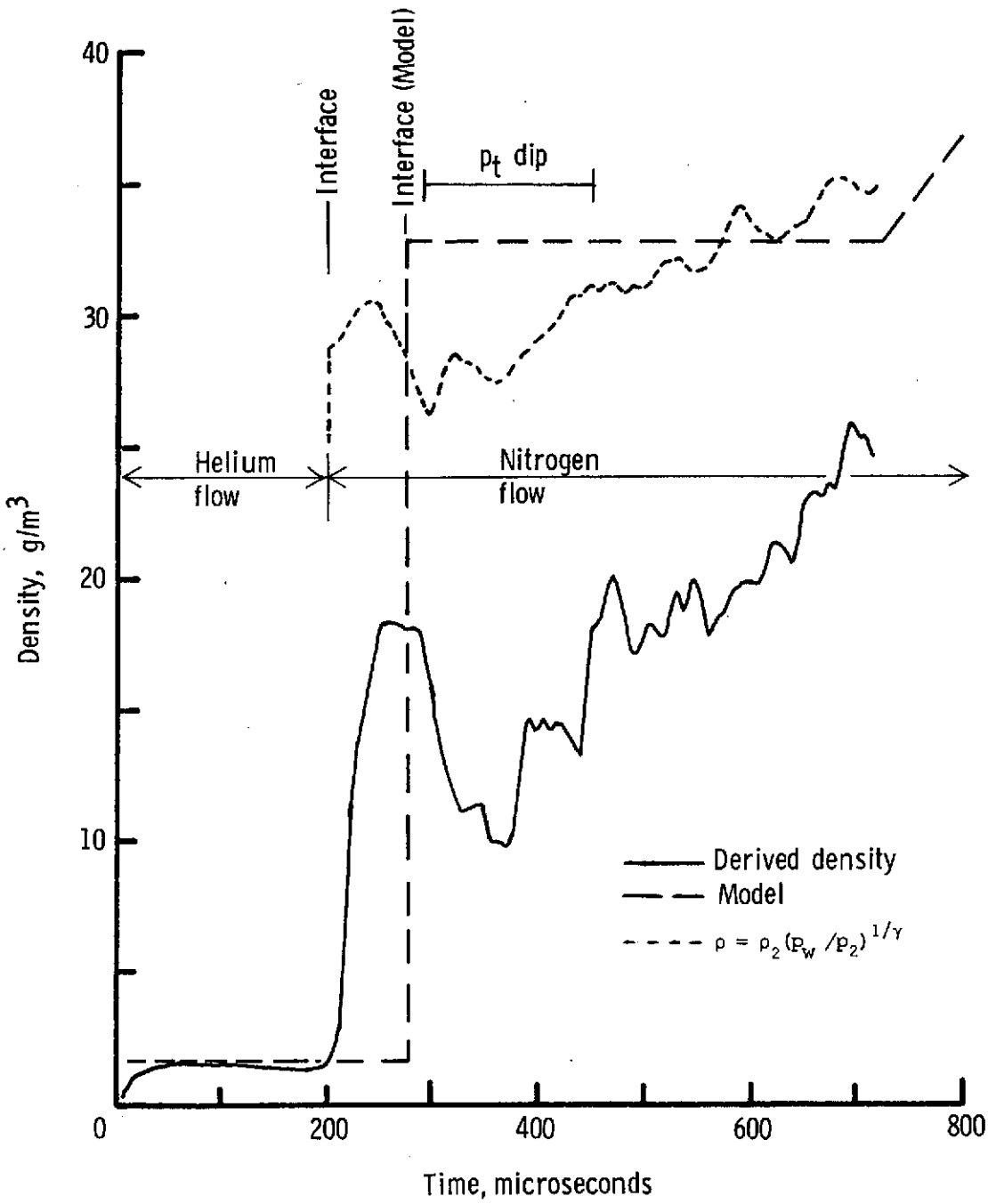

Figure 15.- Density.

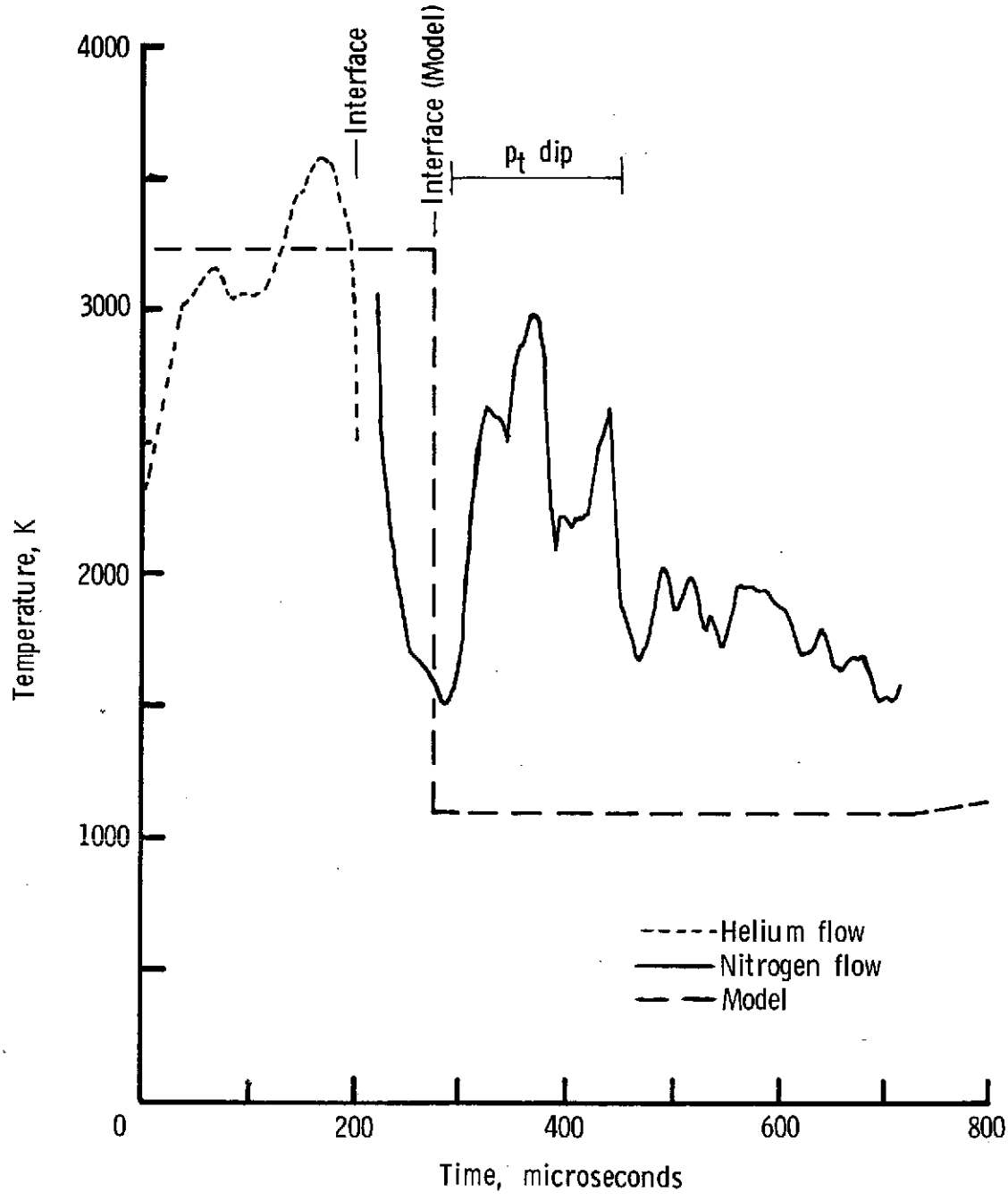

Figure 16.- Temperature.

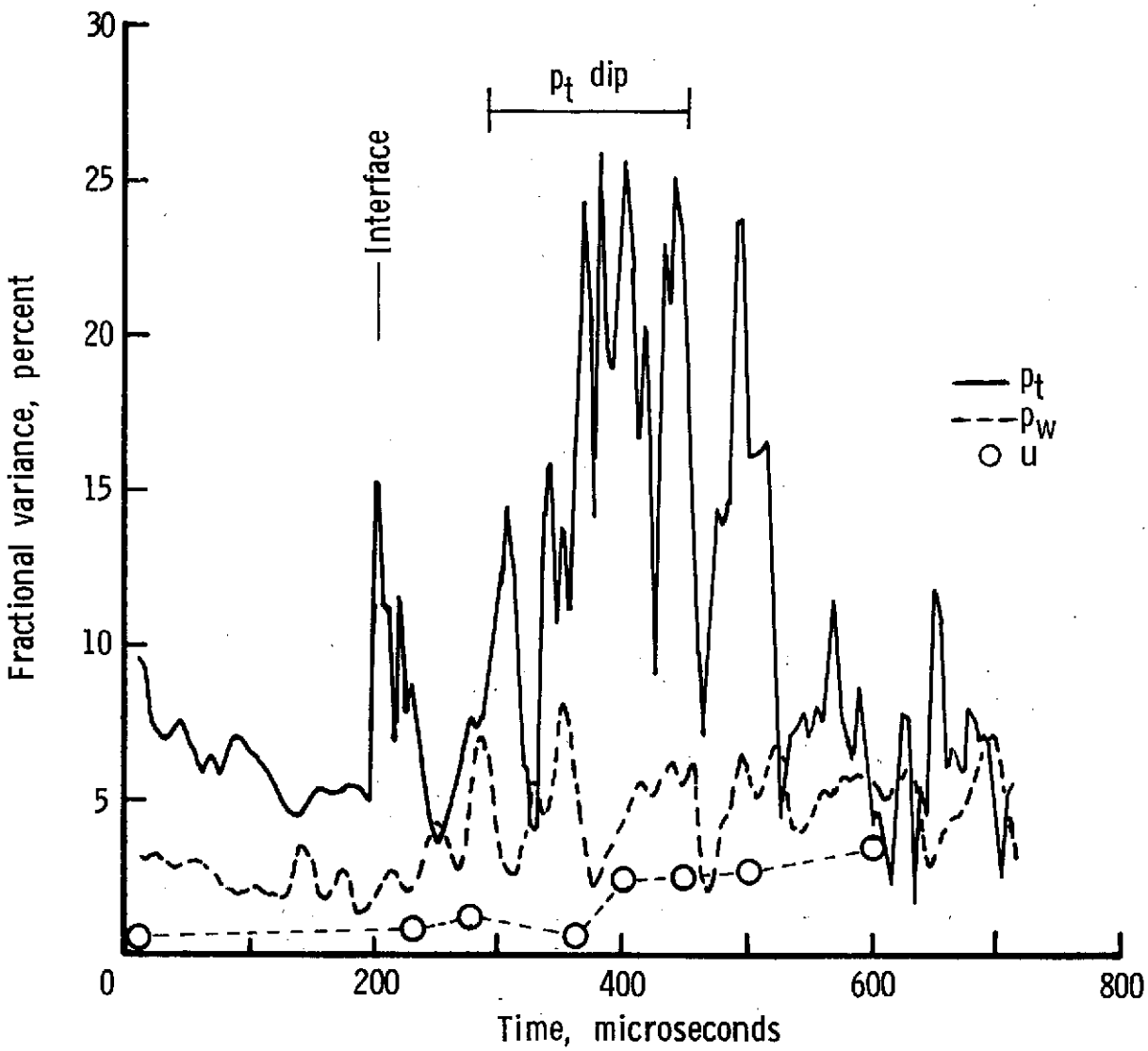

Figure 17.- Variance of pitot pressure, wall pressure, and flow velocity.

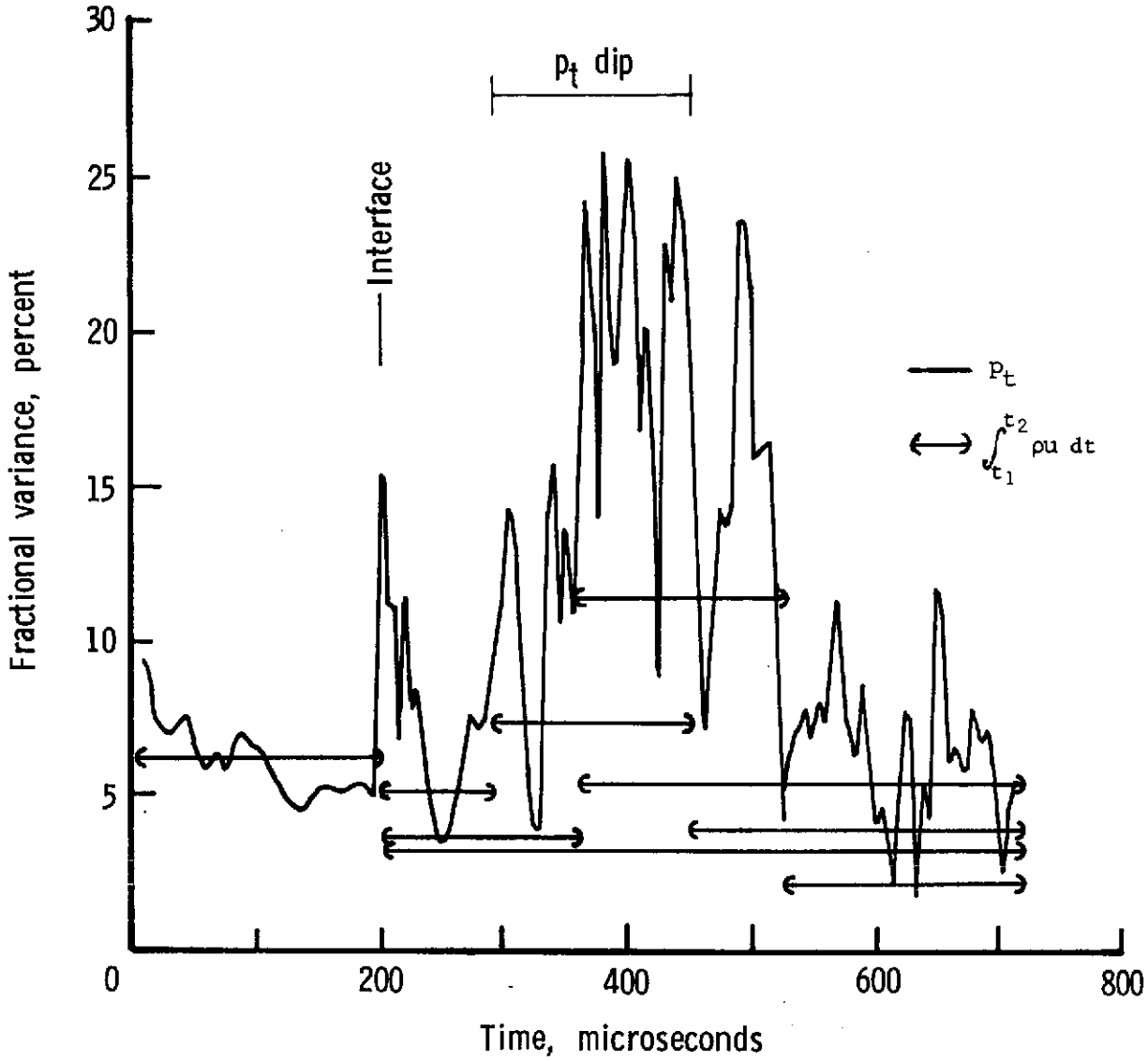

Figure 18.- Variance of pitot pressure and definite integral of mass flux.